An Investigation of Cross-Harmonics as the Cause of Long Secondary Periods in Long Period Variable Stars

by

© **Galina Sherren**

A thesis submitted to the Department of Physics and Physical Oceanography in partial fulfillment of the requirements for the degree of Bachelor of Science (Honours).

Department of Physics and Physical Oceanography

Memorial University

May 2024

St. John's, Newfoundland and Labrador, Canada

Abstract

Long period variables (LPVs) are stars that have ceased burning Hydrogen in their cores and have moved to the asymptotic giant branch [1]. During this phase of evolution LPVs have periods of over 100 days [2]. LPVs can pulsate in the fundamental of overtone modes, and can display multiple pulsation frequencies at once. While the exact driving mechanism of this pulsation is unknown, it is likely that the large convection zone in the star plays into this oscillation period [2]. Some LPVs display a phenomenon called long secondary periods (LSPs) that are 5-10 times the length of the main pulsation period. During the summer of 2023, preliminary analysis to this project involved analyzing the brightness data of a sample of six LPV stars. One of the stars, V CVn, displayed an extra-long secondary period over 30 times the length of the main period of the star. Other stars analyzed also displayed traditional LSPs of 5-10 times the main period. One proposed explanation of V CVn's extra-long LSP was cross-harmonics: the interplay of two simultaneously occuring periods in an LPV. This thesis serves as an investigation of the possibility of LSPs and V CVn's extra-long LSP being caused by cross-harmonics. In order to do this, a stellar evolution models of 0.85 $M_{\odot}$, 0.9 $M_{\odot}$, 1 $M_{\odot}$, 1.2 $M_{\odot}$, and 1.3 $M_{\odot}$ stars were made using Modules for Experiments in Stellar Astrophysics (MESA). These evolution models were then analyzed using GYRE for their pulsation periods during the LPV phase, and the cross-harmonics calculated using python. As a result of this analysis, we do not find evidence of LSPs in the cross-harmonic calculations of the models used for this study. However, periods consistent with LSPs were observed in the pulsation period calculation.

To Mom, Dad, and Nicolai. Love you!

Acknowledgements

I would like to start by acknowledging the guidance and support of my thesis supervisor Dr. Hilding Neilson. Thank you for enduring my endless questions and concerns. This project has been a delight to work on, and I have learned so much through your passion for astronomy. Thank you for your compassion in making astrophysics a more accessible and diverse field.

My friends and group mates Victor Borges, Sashwat Prasadh, Michael Power, and Tashveena Rani Surdha have been immensely helpful with advice, observations, and support.

My friends in the honours room and my classmates have supported me at my lowest, and celebrated with me at my highest.

An additional thank you to Michael Power and Vahid Sheigani for help with the bash and python code.

To my partner, Maddy, thank you for always being there for me during late night writing sessions and early morning exams. Without your endless support I would not be where I am today. Thank you.

To all women and marginalized people in astrophysics that have come before me, thank you for paving the path that I am on. I vow to do my best at continuing to make this field one for everybody.

Table of contents

List of figures

List of abbreviations

HRD	Hertzsprung-Russel Diagram
LPV	Long Period Variable
MESA	Modules for Evolution in Stellar Astrophysics
AGB	Asymptotic Giant Branch
TPAGB	Thermal Pulse Asymptotic Giant Branch
V CVn	V Canum Venaticorum
EOS	Equation of State
ZAHB	Zero-Age Horizontal Branch
PL Relation	Period-Luminosity relation
$M_\odot$	Solar Mass
RGB	Red Giant Branch

Chapter 1

Introduction to Long Period Variables

> "There are more things in heaven and earth, Horatio,
> Than are dreamt of in your philosophy."
>
> -Hamlet, Act I Scene V
> *William Shakespeare*

Although Hamlet was likely not pondering the intricacies of stellar astrophysics, the sentiment still remains true. Stars are much more complex, and all that more eccentric, than any human could fathom. Our knowledge of stellar physics is constantly changing and adapting to advancements in observational technology and modelling capabilities. As a result of this, the field of stellar astrophysics is constantly evolving. I don't doubt that this thesis will one day, either tomorrow or in a decade, become obsolete. Yet it is the endeavour to understand that helps carry collective knowledge forward.

The night sky is home to a multitude of objects that change in apparent brightness over time. These objects can range from asteroids, to active galactic nuclei, to pulsating stars, and are called variable objects. This broad range of objects are separated into categories based on a number of factors, the most important being source of light variation, and type of light curve. A more detailed explanation of variable object categories is demonstrated in the "variability tree" as in fig. 1.1. Variable objects are separated into "intrinsic" and "extrinsic" variables based on whether the variation of

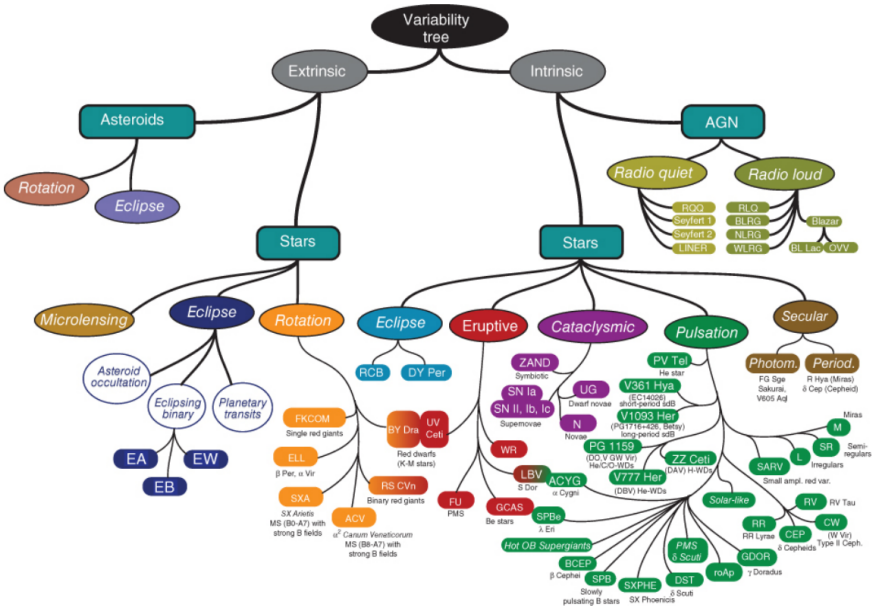

Figure 1.1: Fig. 3.1 of [2], displaying the categories of variable objects in the night sky [2].

brightness stems from the object itself, or an external manipulation.

For the sake of this thesis, the area of interest is intrinsic pulsating variable stars. They reside under the "pulsation" category, meaning they show intrinsic radial and/or non-radial pulsation. The particular type of variable star of interest are Long Period Variables (LPVs), a well-documented but poorly understood branch of intrinsic variable stars. LPVs are separated into two categories: Mira variables, and Semi-Regular Variables (SRVs) [2]. The region of the Hertzsprung Russel Diagram (HRD) where LPVs reside is given in fig. 1.2.

LPVs are low-mass stars that have stopped Hydrogen burning in their core, and moved into the Giant Branches of the HRD [2]. As our sun is a low-mass star, LPVs reflect what will eventually become of our sun in ∼6 billion years. Their evolutionary process is further detailed in section 1.1, and pulsation mechanism during the LPV phase detailed in 1.2. LPV variables are one of the most puzzling stars in the night sky as of today, with the exact driving force behind their pulsation and the cause of their behaviour still being debated. This is counter intuitive, as one of the first variable stars discovered is an LPV called "Mira" or *o* Ceti [1].

Today, we know of thousands of LPVs in the night sky that have pulsation periods

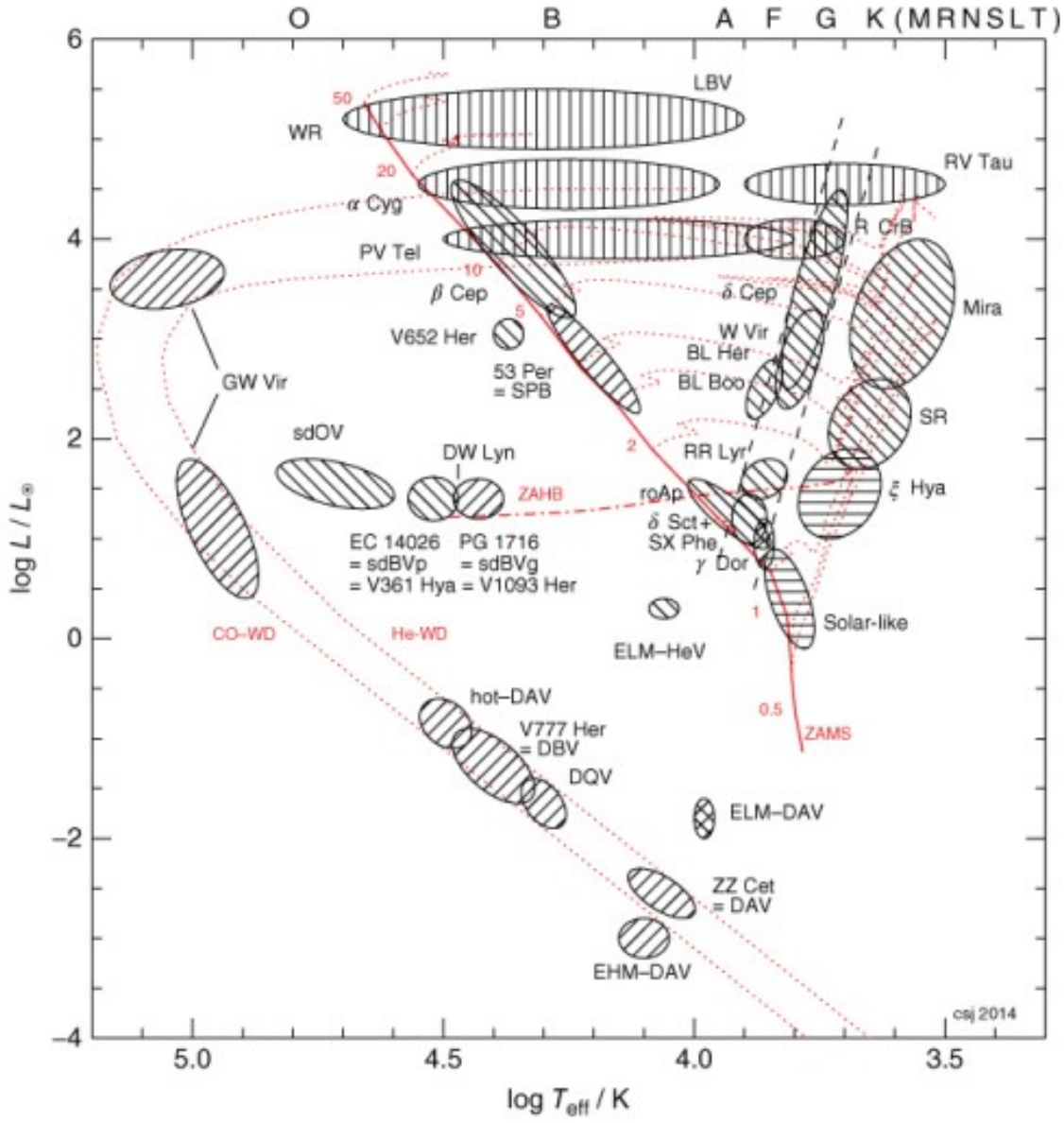

Figure 1.2: Fig. 3.2 of [2], displaying variable star regions on the Hertzsprung Russel Diagram (HRD) [2].

above 100 days. Some LPVs will display an additional variation to their main pulsation period called a "long secondary period" (LSP) that is 5-10 times longer that their main period. Like the nature of LPVs themselves, the reason behind long secondary periods is still a matter of contention. One possibility is that this variation is caused by frequency mixing in stars with multiple periods that occur simultaneously. The purpose of this thesis is to investigate the possibility of frequency mixing as a cause of long secondary periods using stellar evolution models and pulsation frequency calculators. We begin by discussing the evolution of low-mass stars as they are stars become LPVs later in their lifetime. We then move on to some background work performed during the summer of 2023, followed by the methodology. In methods, we discuss the stellar evolution code MESA as well as the complementary code GYRE. Finally, the results and their interpretation is given in section 3.1.2. Example code used for this project can be found in the appendix.

1.1 Evolution of Low-Mass Stars

The cutoff point of when a star goes from a "low-mass" to "intermediate-mass" star is one with contention, with varying cutoff masses cited throughout literature. The textbook "Asteroseismology" by Aaerts et al. considers a main sequence mass of $\leq$ 9 $M_\odot$ to be low-mass, while "Stellar Structure and Evolution" by Kippenhahn et al., considers this limit to be $\leq 2.3\ M_\odot$ low-mass [3] [4]. For the sake of this thesis, we are only interested in stars with a main sequence mass between 0.8 $M_\odot$ to a maximum of 1.3 $M_\odot$.

Fig. 1.3 displays the typical evolution steps of a low-mass star, followed from "Pulsating Stars" by Catelan et al. [2]. While on the main sequence (labelled parts 4 to 5), stars are burning Hydrogen found in their core: if the star is between $0.1\ M_\odot$ to $1\ M_\odot$, the core of the star is purely radiative, while above this mass convection in the core begins taking effect [4][2]. A $1\ M_\odot$ star will spend around 10 billion years on the main sequence, this time varies depending on the mass of the star [2].

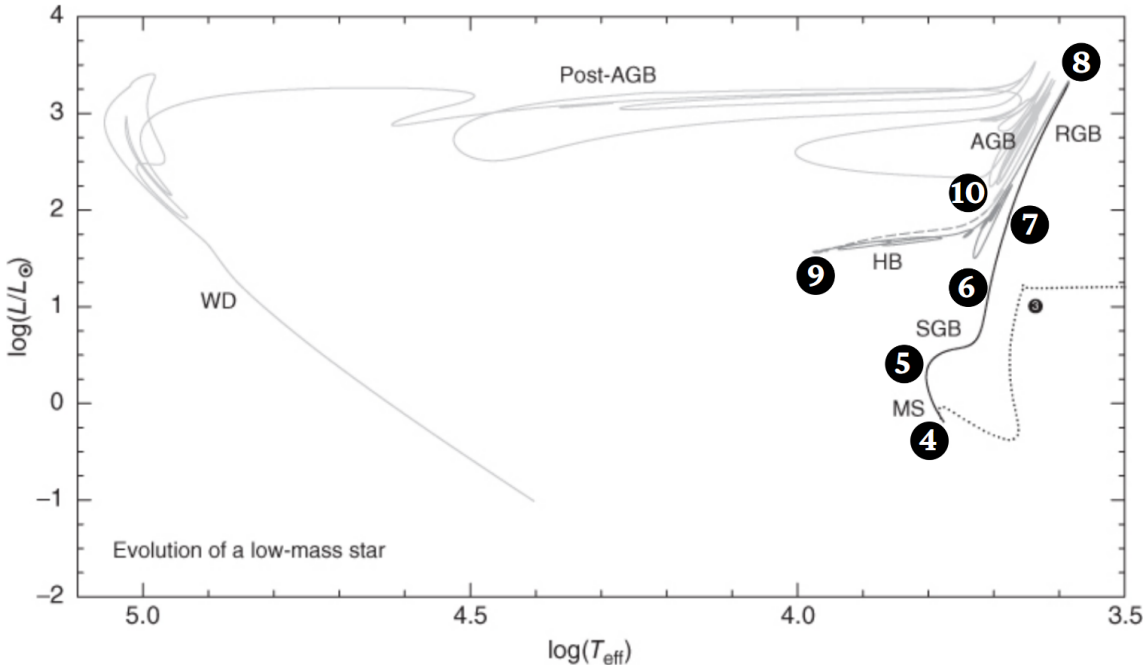

Figure 1.3: Fig. 4.2 adapted from [2], summarizing the evolution track of a low-mass star on the HRD.

Once core Hydrogen is depleted and the star is at the "turn-off point", otherwise point 5 in Fig. 1.3, the core mainly consists Helium obtained through the means of the proton-proton chain [2]. Hydrogen burning is now only taking place in the shell formed around the core, increasing core Helium mass until the "Schönberg–Chandrasekhar" limit causes the core to collapse [2]. Core collapse increases the temperature in the core, the Carbon-Nitrogen-Oxygen (CNO) cycle is now dominant, but Hydrogen consumption continues in the shells, releasing energy that is only partially able to escape the star [2]. The remaining energy causes the star to expand as it reaches the base of the red giant branch (RGB), characterized by a partially degenerate Helium core, with a Hydrogen burning shell surrounded by a convective envelope that is becoming deeper with time [2].

Once the convective envelope reaches a maximum depth, it "dredges up" material from the Hydrogen shell, as Ill as some Helium, in the "first dredge-up phase" indicated by number 6 in figure 1.3. At this point, the convective envelope begins retreating as the H shell and he core increase in mass [2]. Once the evolution reaches point 7, a discontinuity of the chemical composition occurs due to the depth of the convective envelope [2]. This disturbance results in a previously unused supply of fuel to become

available to nuclear fusion [2]. Thus, a reversal in the evolution begins taking place dubbed the "RGB bump" [2]. Eventually this supply runs out and the star continues on its previous path [2].

At point 8 in Fig. 1.3, the star has reached the end of the RGB, where the He core is increasing in mass until eventually the temperature becomes high enough to start burning Helium, also called the "He flash" [2]. It is important to understand that at the point leading up to the He flash, the matter inside the core is degenerate: the nuclear reactions increase the temperature, which in turn increase the reaction rate in a "thermonuclear runaway" [2]. In contrast, non-degenerate conditions allow for a pressure increase that expands surrounding material and cools down the medium in a self-regulating cycle [2]. In degenerate matter a pressure increase is not possible: a local temperature increase does not cause a pressure increase [2]. This degeneracy is important for reasons that will be explained in section 3.1. Many stellar evolution codes struggle to model regions of degenerate matter, which is a fair bit of a star's lifetime.

Once He fusion begins, the star begins its descent through the HRD into the horizontal branch (HB), where the beginning point is called the zero-age HB (ZAHB) indicated by point 9 in fig. 1.1 [2]. Not all stars will have prominent HBs, but the properties of this region holds nonetheless. Cepheid variables, a different type of variable star will become very regular pulsators while crossing the HB. For very low-mass stars ($0.8 to 1.3\ M_{\odot}$), this is not a point of concern as they do not remain on the horizontal branch for long, and are far too low-mass to cause this type of pulsation.

Eventually, just like the star ran out of H to burn in the core, the star will also run out of He, which happens around point 10 in fig. 1.1. this ascent on the HRD is dubbed the "asymptotic giant branch" because it follows close to the RGB region, but will not touch the RGB [2]. The star is home to a non-burning Carbon and Oxygen core but continues to burn He and H in concentric shells outside the core region [2]. It is the AGB phase of Low-mass stars where we see LPV pulsation, the mechanism of this pulsation is described in the coming section. During this era of evolution, LPVs have deep convective envelopes, where convection cells continually stir up material from the depths of the star to the surface [2]. They also have very strong winds: they shed mass at faster rates than other stars and are in fact responsible for a large amount of interstellar dust [2]. This is caused by the loosely attached atmosphere

that can easily become detached during pulsation.

Some stars undergo a "thermal pulse" (TP) on the AGB, which is different from a LPV pulsation, and are caused by ignitions of the H and He shells around the core [2]. The chemical compositions and efficiency of burning can cause the fusion in these shells to die down and re-ignite once they are compressed enough [2]. Because the matter is not degenerate, the temperature does cause an expansion, and thus a visible increase in light we see called the thermal pulse [2].

Beyond the AGB, low-mass stars will "die" by exploding into a planetary nebula, rapidly shedding their mass and leaving a white dwarf in their wake. This section of evolution is irrelevant to this thesis and is left out of discussion.

There are a number of important equations that can be attributed to thermal physics and classical mechanics that describe the stellar evolution we just described qualitatively. Solving these 5 fundamental ordinary differential equations (ODEs) can sufficiently describe the interior of a star. These descriptions follow from section 10.12 of [4]. The first equation, very simply, is a relation between radius and mass. Given by eq. 1.1, r is radial distance from center, m is mass fraction, and ϱ is the density, which allows us to describe a relation between mass and radius [4].

$$\frac{\partial r}{\partial m} = \frac{1}{4\pi r^2 \varrho} \tag{1.1}$$

The next equation is the hydrostatic equilibrium, given by eq. 1.2, which describes the relation that the inward force of gravity needs to be balanced by the outwards radiation pressure [4]. In this equation, P is the outwards pressure, and the term $\frac{Gm}{4\pi r^4}$ is the gravitational effect. The left term being non-zero describes the case where hydrostatic equilibrium is not met [4].

$$\frac{1}{4\pi r^2}\frac{\partial^2 r}{\partial t^2} = -\frac{\partial P}{\partial m} - \frac{Gm}{4\pi r^4} \tag{1.2}$$

The third equation (eq. 1.3) is the change in energy that enters a concentric shell around the center of the star with respect to mass [4]. ε is the energy released per unit mass per second and l is the energy per second entering the shell [4]. The different ε variables are for different sources of energy transfer. ε_v represents energy carried away from the star in the form of neutrinos that are a byproduct of fusion [4]. ε represent

nuclear energy generated and ε_g is a combination of terms of time-dependent partial derivatives that is derived in section 4.4 of [4].

$$\frac{\partial l}{\partial m} = \varepsilon_{\mathrm{n}} - \varepsilon_v + \varepsilon_g \tag{1.3}$$

Next is the transport equation that describes how energy is carried out of the star. Note that this form of the equation is highly generic; ∇ changes depending on the mode of energy transport and location in the star [4].

$$\frac{\partial T}{\partial m} = -\frac{GmT}{4\pi r^4 P}\nabla \tag{1.4}$$

Finally, we need an equation that describes the chemical composition in the star. Eq. 1.5 describes the change in relative fraction of an element with respect to time, where X_i is the relative fraction of an element [4]. The right-hand term describes the rate at which this element is made using the reaction rate of synthesizing this element r_{ji}, and the reaction rate of destroying this element to make a new one r_{ik} [4]. This equation holds for all elements in the star, which seems daunting, but elements heavier than He are so low in fraction compared to H and He that they are commonly grouped together. This approximation calls everything heavier than He "metals" and the fraction of metals in a star the "metallicity" which gives us three chemical composition equations instead.

$$\frac{\partial X_i}{\partial t} = \frac{m_i}{\varrho}\left(\sum_j r_{ji} - \sum_k r_{ik}\right), \quad i = 1, \ldots, I \tag{1.5}$$

Using these five(ish) equations, we are equipped to accurately describe a stellar interior. Note that these equations are a system of non-linear equations that are not straight forward to solve. When talking about modelling stellar evolution, remember these equations, and that by giving some starting conditions we can allow solvers to step through what a star would look like at every point of its life. This is exactly what we will be doing in section 3.1, where we use a stellar evolution code to solve these very equations (albeit in a much more complicated way).

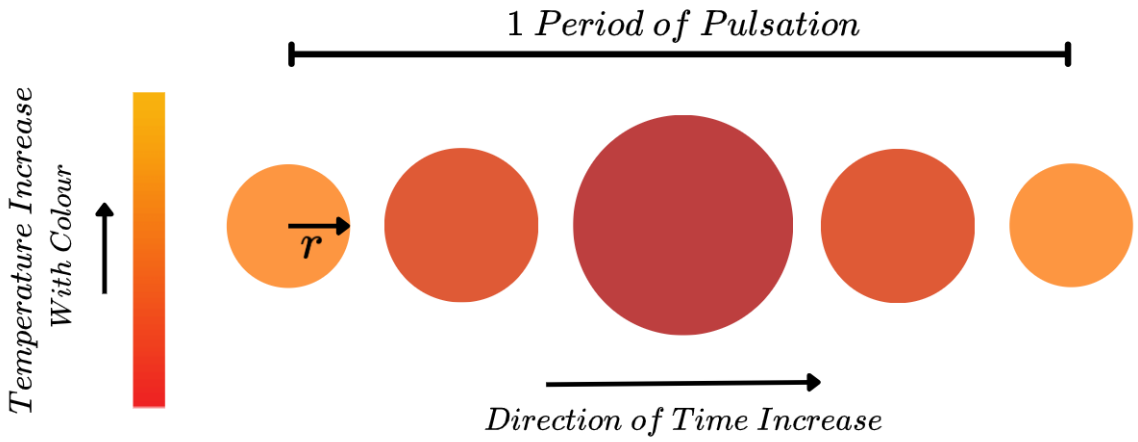

Figure 1.4: A diagram of one period of LPV pulsation, where colour indicates temperature, and r is the radius of the star.

1.2 Pulsation of LPVs

What exactly is stellar pulsation? As seen from fig. 1.2, there are many types of stars that show some kind of pulsation, not all of these stars use the same mechanisms. While we focus on LPV pulsation, it is important to remember that not everything in this section will hold for all types of variable stars.

There are two "types" of stellar oscillation, radial and non-radial, where radial oscillations are spherically symmetric, radial oscillations are not [2]. LPVs pulsate in radial modes; fig. 1.4 summarizes the radial pulsation of an LPV. At maximum light the star is smaller, but hotter (denoted using colour), and at minimum light the star is larger but cooler [2]. This variation is the one we see when we look at optical wavelength light curves of an LPV over time. Although Miras and Semi-Regular Variables (SRVs) are different categories, there is no discontinuity in the HRD where SRVs stop and Mira variables begin. We will discuss the difference between these two categories but the mechanisms are still valid for both.

Radial oscillations in stars are caused by sound waves resonating in a star: matter gets compressed, sending shock waves through the star. Because of this, we can use properties of sound travelling though different media to model how pulses would travel in a star. The pulsation period Π, can be obtained using the adiabatic sound speed obtained using the bulk modulus:

$$v_s = \sqrt{\frac{\gamma P}{\rho}} \tag{1.6}$$

where P is the pressure, obtained from the hydrostatic equilibrium in eq. 1.2, γ is a constant specifying an equation of state, and ρ is a constant density [1]. Then applying some boundary conditions, we can obtain an expression for the period given a certain γ and ρ (for a more detailed explanation, see section 14.2 of [1]). This relation is derived from equations 1.1 through 1.5, or the equation required to model a star. However, it makes some assumptions of an adiabatic environment and constant density throughout the star. The consequences of these assumptions are discussed in section 3.1. An adiabatic approximation means there is no transfer of heat between the shells of a star. Stars, of course, are not actually adiabatic, but this approximation is used with justification also discussed in section 3.1.

We can think of the sound wave analogy as a taught string: when plucked, a taught string will oscillate at a certain frequency and will have harmonics, or "overtones" that correspond to different frequencies. Certain frequencies will cause standing waves in a string, exactly like the radial modes of a star. The translation of this analogy to a star means that there is a fixed node at the center of the star, and an open end at the star's surface where the gasses can freely move. The fundamental mode is the frequency which all gas in the star moves in the same direction, there is no node [1]. The first overtone has one node, the second overtone two, and so on. Fig. 1.5 displays a diagram of this motion.

MACHO and OGLE database studies of LPVs have concluded that Miras are fundamental radial mode pulsators, and SRVs are fundamental, 1st, 2nd, and 3rd overtone pulsators [5]. SRVs can also pulsate in multiple modes at once, causing a "beating" phenomenon, which will be explored more in section 2 [6].

At this point, we understand what the pulsation looks like, but what drives this pulsation? There still needs to be some mechanism perturbs the star to cause a pulse. The exact mechanism for LPVs is not well understood, but there are a few possibilities that could contribute. The answer likely lies within the interplay between convection and pulsation [2]. If you are familiar with Cepheid variables, or more "classical" pulsators, you might be familiar with the opacity mechanism, also called the κ mechanism. This mechanism involves the medium of the star becoming optically

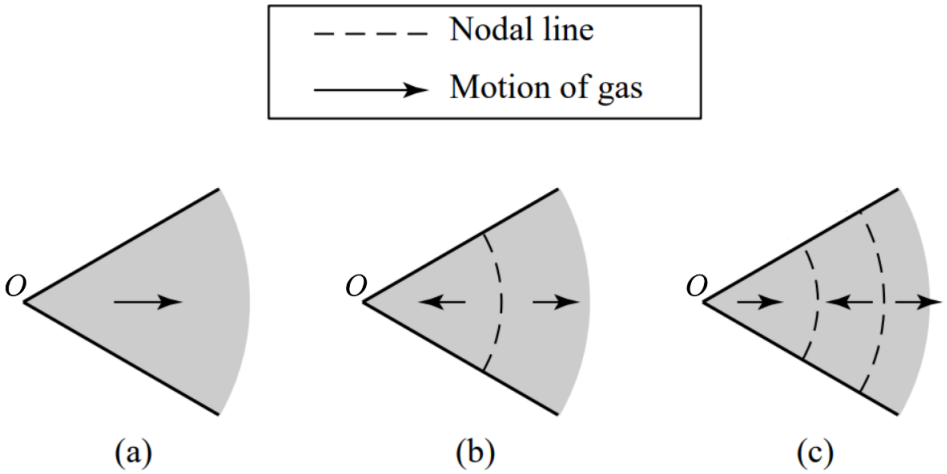

Figure 1.5: A diagram of radial pulsation where (a) corresponds to the fundamental mode, (b) corresponds to the first overtone, and (c) corresponds to the second overtone [1]. O denotes the center of the star. The figure is adapted from fig. 14.9 of [1].

dense to photons streaming out of fusion regions, and building pressure until it is strong enough to push outwards [1]. However, this mechanism is only efficient in regions where radiative energy transport is more efficient. We cannot apply the same principles to largely convective stars like LPVs [2]. This has been a widely studied topic in stellar physics, for a more detailed explanation of the various studies and their conclusions, refer to section 8.1 of [2].

As of today, there is no exact consensus on the driving mechanism, only that the coupling between convection and pulsation replaces traditional drivers like the κ mechanism in traditional pulsators [2] [7]. Many models tried for LPVs cannot fully account for the large amplitude and long periods of pulsation simultaneously. For this reason, models that treat LPVs using schemes of pulsation that are solely based on pulsation drivers applicable to classical pulsators must be treated with caution. This reality also applies to this thesis.

1.2.1 Long Secondary Periods

Long Secondary Periods (LSP) are a phenomena observed in about one third to a half of LPVs, and are an additional type of variability aside from main periods that occur in the LPV phase of evolution [8]. LSPs are typically 5-10 times longer than the main pulsation period, where the main period is defined as the period with the

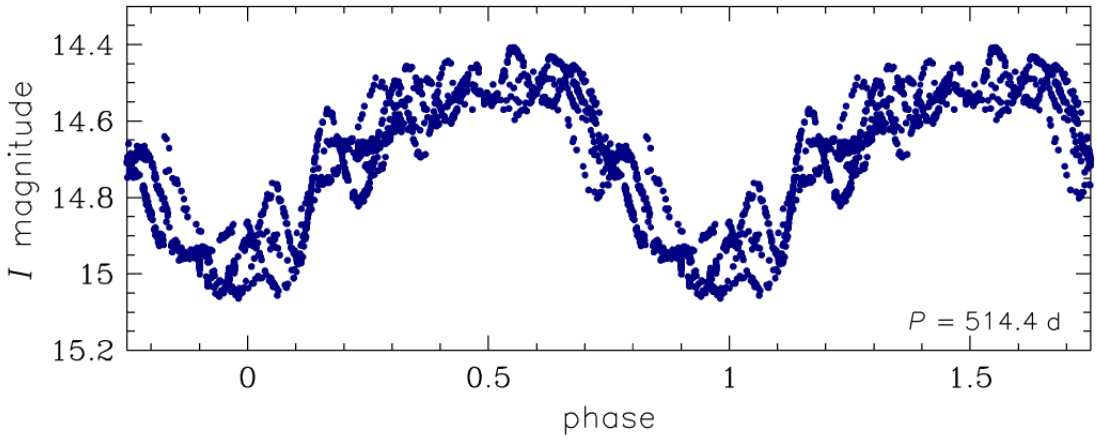

Figure 1.6: Adapted from fig. 7 of Soszyński adn Udalski (2014) displaying an example light curve of an LSP star folded and phase-matched [10]. The main period variation is clearly visible as a short period variation inside the larger-period LSP. The light curve is sampled from OGLE I-band light curve from a star in the Galactic bulge [10].

largest amplitude [9]. Fig. 1.6, adapted from [10] displays a sample light curve of an LSP star, folded so that the phases align. While the astronomy community has been aware of the phenomenon of LSPs for over a century, the underlying mechanism is highly debated, with different studies attributing it to different causes [11]. In their 2015 paper, Saio et al. investigated oscillatory convective modes as the cause and found that the resulting oscillation "roughly" agreed with the properties of an LSP [11]. They did indicate that the models used were cooler than that of the AGB stars used as a blueprint, and concluded that a more sophisticated convection model was needed to verify any findings from the study [11].

The most recent study on LSPs was done by Soszyński et al. in 2021, where they investigated a binary companion as the reason for LSPs [12]. They found secondary eclipses visible only in infrared wavelengths in around half of a sample of 700 LSP variables [12]. They attribute this to a system of a dust cloud orbiting the variable star alongside a companion substellar or stellar object [12]. While an excellent analysis, there still remains some questions with this conclusion: for this to be possible, a large amount of binary systems would have to be seen face-on, but no such discoveries have been made [13]. This issue among others have left the astronomy community with great guesses, but no concrete evidence as to the origin of LSPs.

During summer of 2023, my research under Dr. Hilding Neilson prompted the

analysis a sample of 6 LPV stars. This research is further detailed as background in section 2. Many of these stars displayed an LSP, but no concrete reason behind most of the LSPs were found, partially due to lack of observational data. As a result of analysis, we did find LSP-like periods in most stars, but these LSPs were much longer than 5-10 times the length of the main period. One of the stars analyzed, V Canum Venaticorum (V CVn), displayed an extra-long secondary period, which Kiss et al. (2000) argues is due to cross-production [6]. While they do not elaborate on their definition of cross-production, it can be inferred that they refer to frequency-beating or cross-harmonics that can be described with :

$$f_{mixed} = f_1 \pm f_2 \tag{1.7}$$

where the added and subtracted values of two frequencies that occur simultaneously cause f_{mixed}.

1.3 Goal of the Study

Having contextualized LPVs and LSPs I can now further explain the goals of this study. Despite the underlying mechanism for LSPs being highly debated, an argument for frequency mixing can be made. The goal of this study is to model LPVs and calculate the pulsation frequencies using a stellar modelling code to understand if frequency mixing is the potential cause for LSPs. The software, parameters, and calculations used are discussed in section 3.1. We expect that multiple frequencies will occur at the same point in evolution, but we may not observe frequencies consistent with an LSP. Luckily, we have observational data from LPVs that we can compare these models to. The analysis of the observational data used to justify this study is discussed in the next section, and this data will be directly compared to the results of the models.

This thesis also partially serves as an investigation of whether MESA and GYRE are capable of computing the periods of LPVs. Masses as low as 0.85 $M_\odot$ have not been attempted to be modeled in literature using the methods we employ in this thesis. Thus achieving a viable model would be a novel endeavour.

Chapter 2

Background

The American Association of Variable Star Observers (AAVSO) is an organization dedicated to collecting and cataloguing data from variable stars in the night sky. Contributions to data can be made by amateur and professional astronomers alike, as continuously tracking thousands of variable stars as they change in brightness is not an easy task for a small group of people. Their archive of observations span over a century, and prove exceptionally useful when trying to understand LPVs: in order to deduce the periods or track the evolution of their pulsations, observations spanning multiple times the length of one pulsation cycle is needed. This can be multiple years for some stars, and in the case of LSPs, a few cycles could mean a decade.

From May to September of 2023, I worked under Dr. Hilding Neilson, where I used Fourier analysis and Wavelet analysis techniques to analyze time series data of 6 LPVs. Because this work was not in fulfillment of the B.Sc. Physics (Honours) degree at Memorial University, it is not discussed in depth in this thesis, but will be submitted for journal publishing under citation [14] and is currently a work in progress. For further explanation of this study, consult this resource.

The 6 stars studied were V canum Venaticorum (V CVn), UZ Aries (UZ Ari), AK Pegasus (AK Peg), RX Boo (RX Bootis), Z Ursa Majoris (Z UMa), and L_2 Puppis (L_2 Pup). The data is in the optical wavelength and is designated as high-quality data by the AAVSO, and is in the form on light curves, or magnitude vs. time graphs as given in fig. 2.1. The data analysis and visualization program used is AAVSO's program VSTAR [15].

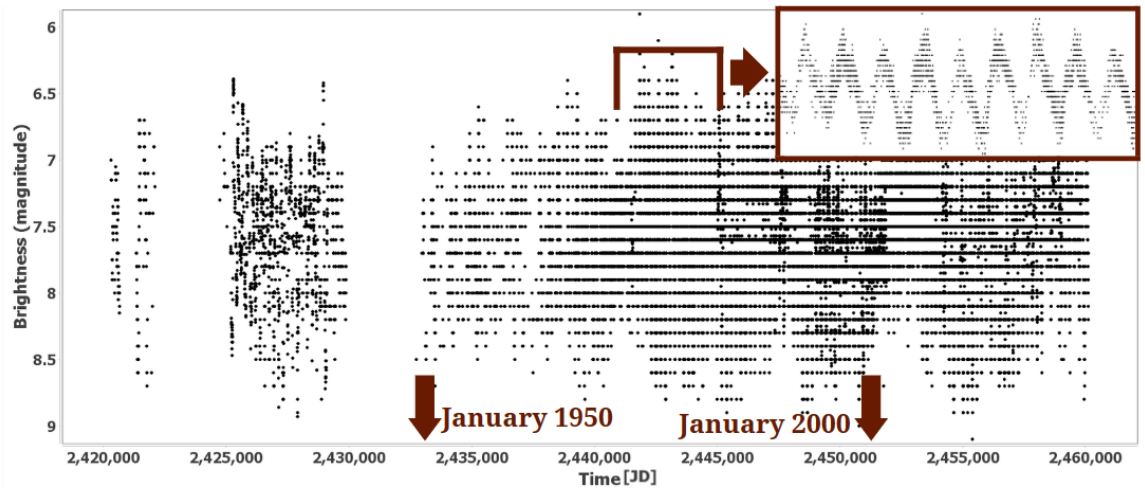

Figure 2.1: The light curve of LPV V CVn in the form of brightness [mag] vs. time [JD]. The highlighted region clearly displays the periodicity in the light curve [16].

By applying Fourier analysis, we obtain a power vs. frequency graph that indicates the statistical significance of each frequency analyzed. The result of performing Fourier analysis on V CVn's light curve is given in fig. 2.2. From the significant periods, we observe four closely-spaced periods around 190 days, of which the lower significance ones are a result of variability in the periods. The two main periods of V CVn are 192 and 186 days, and these periods are consistent with those in literature. We also observe a 5407-day period that is not mentioned in literature. However, comparing this study's analysis to that of fig. 2.3, the 5407-day period seemingly correlates to the $f_0 - f_1$ period that Kiss et al. point out [6]. This period is much longer than a traditional LSP which is 5-10 times longer than the main periods of a star. The 5407-day period is over 20 times longer than V CVn's main periods, making it either an unlikely candidate for a traditional LSP, or one of the highest LSP to main period ratios among LSP stars. Aside from V CVn, the remaining 5 stars also showed multiple periods with some LSPs and contenders for extra-long cross-harmonic frequencies.

It is important to note that the Fourier spectrum is far less noisy in this study's analysis. This is likely due to Kiss et al. performing their analysis around 2000, while our analysis takes place over 20 years later. In this time, there has been much contribution to V CVn's observational data, which would allow for better constraints on the Fourier spectra.

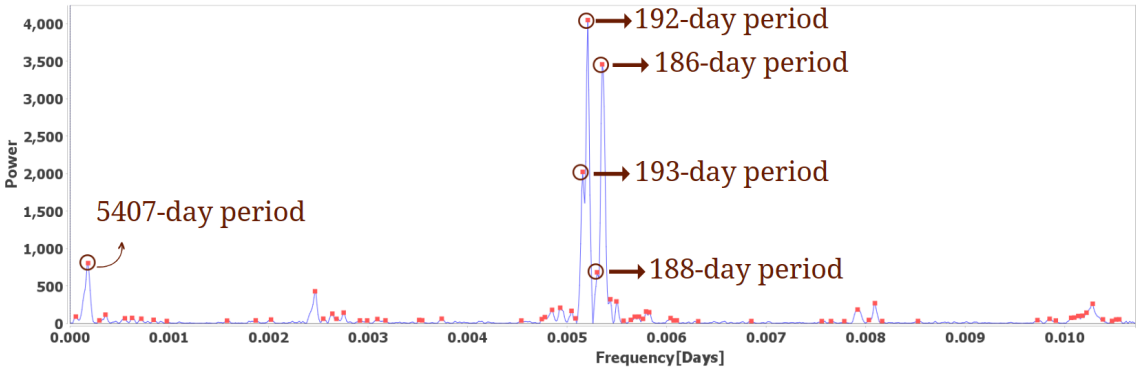

Figure 2.2: The result of performing Fourier analysis on V CVN's light curve in the form of a power vs. frequency graph. The most significant periods are indicated on the graph.

Another important point to consider is that this period could simply by an artefact caused by the Fourier analysis: in time series data it is not uncommon to observe false peaks for a number of reasons. One of these artefacts is "aliasing", and are a result of performing Fourier analysis on data with a limited number of sampled points [17]. This results in false peaks that are not in fact present in the star's pulsation [17]. Using techniques such as residual analysis, it is easy to determine these false peaks, which we do in V CVn's case. In some cases, this can present as symmetric peaks mirrored around the main periods. Looking at fig. 2.2 we do see peaks surrounding the main periods that are in symmetric locations, however, the peak at around 0.01 days does not have a symmetric power as the 5407-day period. For this reason, there is a non-zero chance that this peak is not simply an artefact of data analysis but occurring in the star itself.

It is not clear what Kiss et al. mean by "cross-production", the theoretical background is missing from the paper. It is likely that they are referring to "cross-harmonics", which are real frequencies occuring in a star and are a linear combination in a multi periodic star. This can be described with the equation:

$$f_{jk} = jf_1 + kf_2 \tag{2.1}$$

where j and k are integers [17]. This is likely the reason they write off the 5407-day period as an artefact such as in eq. 1.7 and fig. 2.3 but is in fact a real phenomenon. There are multiple stars that exhibit this type of variation, of one example is TU

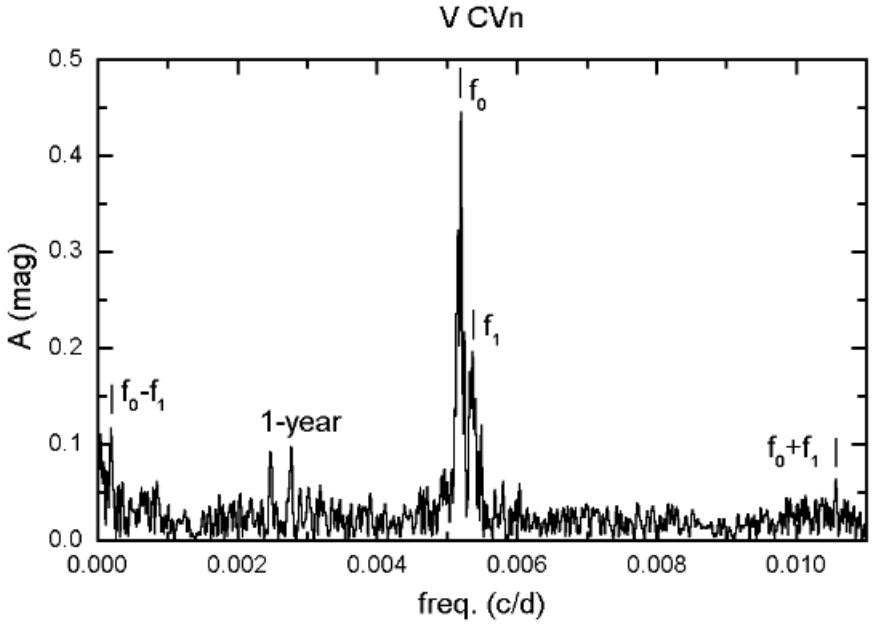

Figure 2.3: A different Fourier analysis of V CVn's light curve performed by Kiss et al. (2000). The image is taken from fig. 5 of [6].

Cassiopeia (TU Cas) where currently 25 cross-harmonic periods have been observed occurring in the star [17].

While TU Cas is a Cepheid variable, the principle of cross-harmonics are applicable to any star that displays multiple periods that are distinct and not a harmonic of one another [17]. For this reason, we will be applying this formula to the calculated frequencies of pulsation using stellar modelling codes to determine if LSPs or even an extra-long LSP such as V CVn's could be caused by cross-harmonics.

Chapter 3

Methods

As this is an experimental project, I require a method to model LPVs, and then calculate the periods that occur at different points in their evolution. There are a plethora of coding suites and programs that allow for users to obtain stellar models, one of the most prolific being "Modules for Evolution in Stellar Astrophysics", or "MESA" [18][19][20][21][22]. I also utilize the MESA-compatible stellar pulsation calculator "GYRE" to then calculate the radial pulsation periods during various points in the stars' evolution [23] [23].

The method utilized for calculating the radial stellar pulsation frequencies in GYRE requires an initial input in MESA file format. This is done through obtaining a stellar evolution track on the HRD and then inputting detailed information about the star at one age point into GYRE to calculate the eigenvalues (which are the frequencies) of the stellar pulsation equations. This two-step process is then finished by plotting and analyzing the data in Python. I discuss this process in further detail in the remainder of this chapter, beginning with the MESA evolution tracks.

3.1 MESA

"Modules for Experiments in Stellar Astrophysics", or MESA, is a FORTRAN 95 based open-source code developed to make stellar models, and can model a variety of stellar phenomena [22][24]. The development was fronted by Bill Paxton but has many more contributors than can be done justice in one sentence [22][21][20][19][18][25]. It

is a collection of modules that allows the user to perform a variety of experiments ranging from calculation stellar evolution tracks to obtaining theoretical light curves [24]. We utilize MESA to calculate the evolution tracks of the stars with the desired initial mass on the HRD, which can then be input to GYRE. The process of calculating these tracks is discussed in section 3.1.2. The numerical methods are briefly discussed in the following section; more detailed information about the operation of MESA can be obtained from the MESA release papers [22][21][20][19][18][25], and the MESA website [24].

3.1.1 Numerical Methods

While the focus of this project is not the computation, the process is briefly described in this section; more detailed solver schematics can be found in the MESA release papers, namely [22], [21], [20], [19] and [18]. MESA uses a Newton-Raphson solver to find the multidimensional, nonlinear roots of the stellar system and advance the evolution of a stellar model [22]. The basic equation is given in eq. 3.1, where y_i is a trial solution taken from the previous iteration of the model that has been modified using evolution conditions [22].

$$0 = \vec{F}(\vec{y}) = \vec{F}\left(\vec{y}_i + \delta\vec{y}_i\right) = \vec{F}\left(\vec{y}_i\right) + \left[\frac{d\vec{F}}{d\vec{y}}\right]_i \delta\vec{y}_i + O\left(\delta\vec{y}_i{}^2\right) \tag{3.1}$$

In this equation, $\vec{F}_i$ is a residual, $\delta\vec{y}_i$ is the correction, and $\frac{d\vec{F}}{d\vec{y}}$ is a Jacobian matrix [22]. The solution for the properties of the stars are reached through iteratively improving the trial solutions until one is accepted when it meets a set of convergence criteria [22]. In most cases, the trial solution is reached relatively quickly in one or two iterations, aside from complex evolution regimes such as the onset of He flash [22]. If the first iteration does not have satisfactory residuals, the program reduces the timestep and tries again [22]. In essence, if the properties of a star change "too quickly", the program reduces the time in between steps to ensure the changes are recorded properly. "Complex evolution regimes" in this case refers to where the system is highly nonlinear, and the program is driving the time step to lower and lower values. A lower timestep limit can be given to the program that will terminate the run if reached [22]. Given that we are calculating stellar properties well into He

flash this does become a issue. To get around this we simply set a lower timestep limit and allow simulations to run for longer times.

3.1.2 Calculating the Evolution Tracks

As the initial mass function of stars dictates, more low-mass than high-mass stars form when interstellar dust begins collapsing [1]. For this reason, combined with the knowledge of which stars tend to go into the LPV regime, we select $0.85, 0.9, 1, 1.1, 1.2, 1.3\ M_\odot$ for investigation. The reason $0.85\ M_\odot$ and not $0.8\ M_\odot$ was used is due to MESA having issues reaching convergence at degenerate regimes in very low masses. we limit the maximum mass at $1.3\ M_\odot$ due to time constraints, as well as uniformity in schemes used during evolution. The same schemes were applied throughout these mass models, and only initial mass, time step limits, and model number limits were changed. Varying the mass a large amount from the default of the test suite could cause improper parameters to be used for these lower masses. We also only calculate 6 evolution tracks due to the short timeline of this thesis, as each evolution run takes anywhere from 2 to 4 hours.

MESA uses a number of modules that calculate different variables in a star: the modules we use are the opacity (kap), equation of state (eos) modules. Recalling the equation of state from section 1.1, we need to be able to define a state for the material inside the star: it may not necessarily follow the ideal gas relation. The eos module will determine which inputs to use for the equation of state of the material depending on the location and properties of transition regions in the star [24]. Similarly, the kap module combines the opacity data and determines which sources contribute to the overall opacity, and the location of blends between them [22]. Finally, there are other controls that can be used to determine initial mass, limits of timesteps and model numbers, mixing length parameters, and more. The controls that tell MESA what parameters and calculation schemes to use are stored in namelist files that can be edited by the user to suit the needs of the project. The same overshooting, mixing length, mass loss, and metallicity were used for all masses, for which an example can be seen in A.

The calculation scheme was based on the MESA test case which evolves a $1\ M_\odot$ from pre-main sequence to the formation of a white dwarf. We altered this test suite to cut out the pre-main sequence and post-termination point AGB (TPAGB)

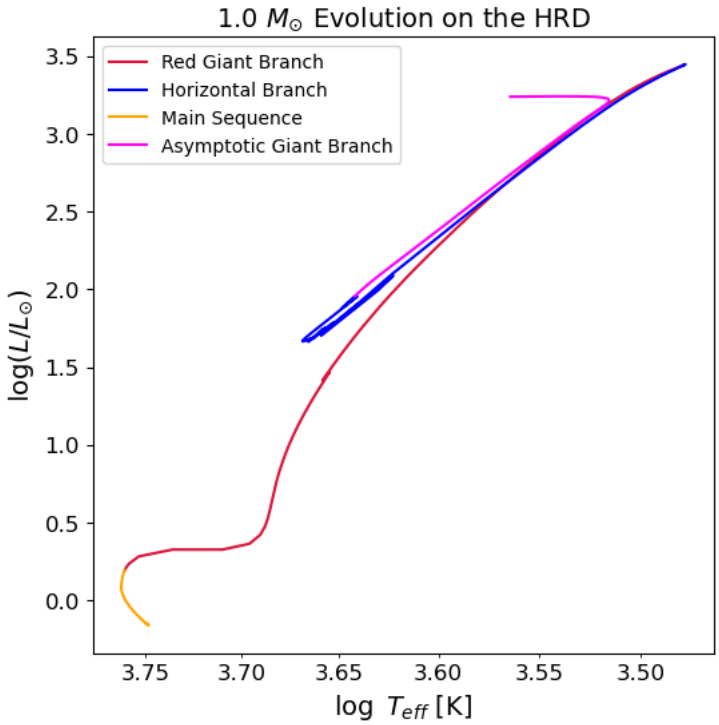

Figure 3.1: The evolution track of a 1 $M_\odot$ star using MESA displaying the different regions of evolution schemes the code uses.

calculations, and varied the initial mass in the namelists for each respective mass being modelled. This evolution module uses separate calculations for each region of the HRD that uses different schemes to evolve (e.g. core H burning, core He burning, shell H burning). The different regions are demonstrated in figure 3.1. Aside from the main sequence, each section used the last values of the previous section and then continues the evolution using the new commands. To determine where to end a section and start the next one a variety of commands were used, which can be seen in Appendix A.

As MESA calculated the evolution tracks, for every 10 models generated, a "profile" file was output. These are a detailed summary of around 100 of the stars parameters at a single timestep. Profile files are readable by GYRE, and are used in the next step of the process in calculating the pulsation periods. During the AGB phase, the frequency of outputting a profile file was increased in order to get higher-resolution period calculations in the next step. This was taken from outputting a profile file every 10000 models, to every 10 models. In some circumstances, the resolution was

changed after a first evolution track run, and the run resumed using the "./re xphoto" command. This does not cause a change in any of the evolution tracks greatly, it just increases the resolution so the evolution track is more detailed. An example of this is given in fig. 3.2, where the high resolution is apparent though the existence of curves rather than lines. The overall shape is preserved, but the exact location on the HRD becomes much more refined.

3.2 GYRE

To obtain frequencies of the pulsations of stars modelled using MESA, we rely on GYRE: a stellar oscillation code that is compatible with MESA models [23]. GYRE solves the fundamental stellar pulsation equation using the "Magnus Multiple Shooting" scheme for solving linearized pulsation equations, and is written in FORTRAN 2008 [23]. The compatibility with MESA allows for the previously calculated stellar evolution tracks to be input and the pulsation frequencies calculated based on the profile read into GYRE. While there are multiple ways of taking MESA-calculated evolution models and calculating stellar oscillation parameters using GYRE, we rely on the method outlined by the example walkthrough outlined on the GYRE website [26].

The walkthrough method is not adapted to handle large inputs of profiles from evolution track calculations at once, and requires manual input of each file. To avoid this inconvenience, we write a namelist with desired parameters as indicated in the walkthrough, and place all profile files in both GYRE and data file format in the same directory. We then employ a bash script to cycle through each profile and output the pulsation frequency, χ^2 value, radial order, and number of iteration the code loops through before achieving a desirable result. This data was then read into Python for plotting using the Python packages PyGyre and Mesa Reader [27] [28].

3.2.1 Numerical Methods

Actually modelling stellar pulsation is not very different from modeling evolution, except the time scales of calculation are much shorter. Recall the taught string analogy from earlier. Mathematically this can be described with the wave equation that can

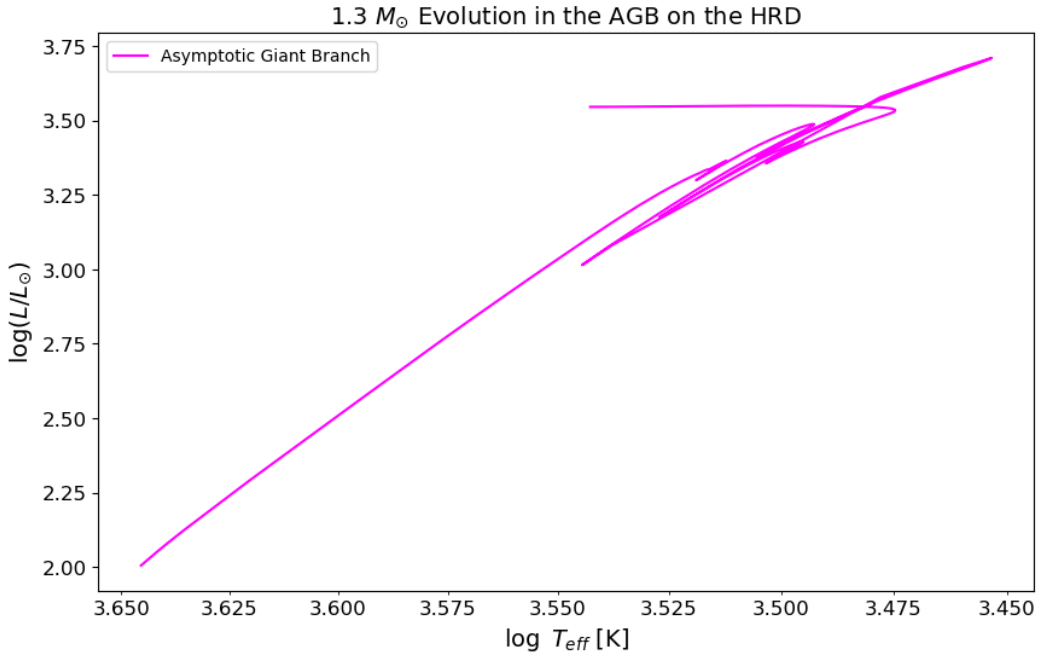

(a)

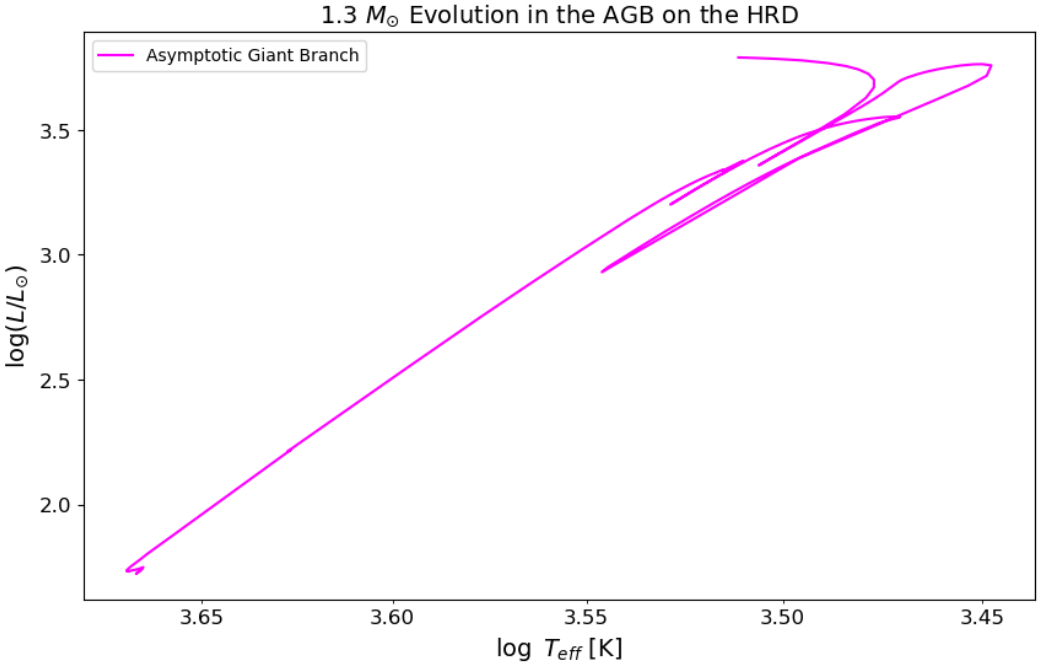

(b)

Figure 3.2: The evolution tracks of a 1.3 $M_\odot$ star in the AGB region with a low resolution (a) and a high resolution (b).

be numerically solved for its eigenvalues and eigenvectors describing the modes of oscillation in the string. This is similar to what GYRE does with stellar oscillation [23]. GYRE begins with a radial displacement perturbation trial solution ξ_r of the form:

$$\xi_r(r,\theta,\phi;t) = \mathrm{Re}\left[\sqrt{4\pi}\tilde{\xi}_r(r)Y_\ell^m(\theta,\phi)\exp(-\mathrm{i}\sigma t)\right] \tag{3.2}$$

The ordinary differential equation (ODE) governing radial displacement is than discretized on a spatial grid decomposing them into a system of first-order ODEs. These equations are then solved in a matrix for their eigenvalues, which yield the frequencies of oscillation. As mentioned previously, the focus of this project is not the computational methods of the coding suite, and more information can be learned about GYRE from [23] and [26].

3.2.2 Pulsation Frequencies Calculation

In order to calculate the pulsation frequencies, the profile files from MESA are read into the GYRE file directory. Then using a bash script file, a command is executed to cycle through all profiles and calculate the corresponding fundamental, 1st, 2nd, 3rd, and 4th overtone modes at each point. A range of 100 days to 10000 day periods are specified as a search range, only in the radial mode of $l = 0$. Both the adiabatic and non-adiabatic cases of pulsation frequencies are calculated. Non-adiabatic cases of pulsation are more complicated to solve, the method of this calculation if described in [26]. Non-adiabatic cases are useful when dampening or growth of modes are of interest. Calculating the non-adiabatic case requires non-adiabatic effects being included in the oscillation equations, and are outlined in [23]. In essence, accounting for non-adiabatic effects will yield calculations of amplitude of period so rates of change of periods can be detected. The adiabatic case yields the frequencies with the same amplitude throughout, so the same period change rate calculation cannot be performed. While this is not the purpose of this project, the non-adiabatic case is calculated for the sake of comparison between methods and computational rigor.

Once the calculation command is executed, GYRE begins dumping the data in the terminal and in log files that can be read into Python using the package PyGYRE [28]. An example frequency calculation is given in fig. 3.3. Following this, each period was

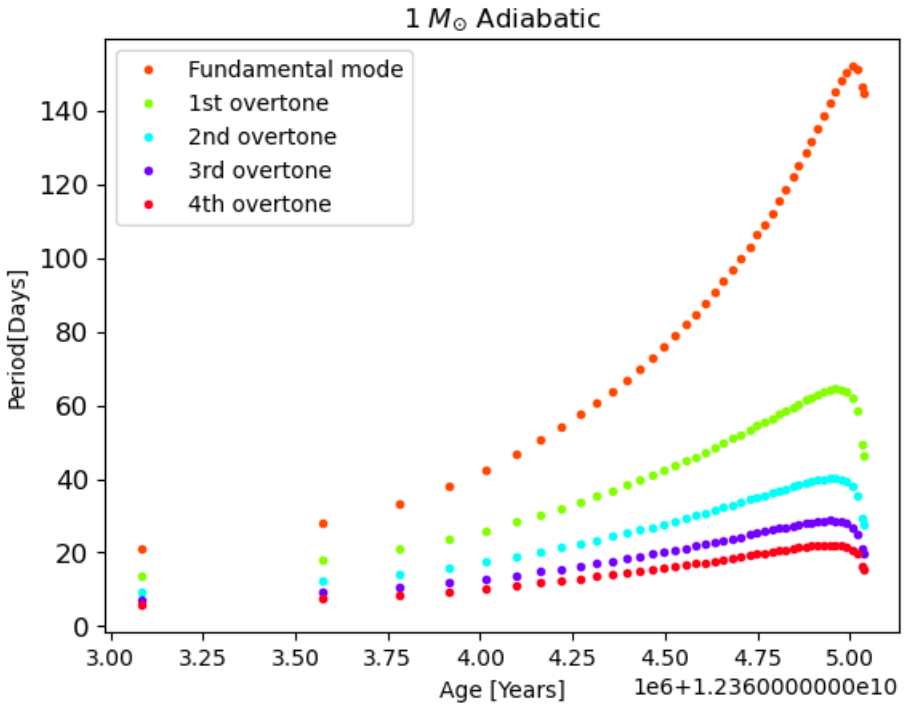

Figure 3.3: Result of adiabatic period calculations of a 1 $M_\odot$ star in the AGB region of evolution.

subtracted and added to each other to form a linear combination of frequencies. Note that from eq. 4.1, the linear combination can occur with different integer coefficients of the frequencies being added. There is no way of determining the boundaries of what maximum coefficient to use; in the case of TU Cas, there were 25 cross-harmonics. Setting an upper limit would be purely based off a guess, and for this reason only the case of $j = 1$ and $k = 1$ for eq. 4.1 is considered. This is also consistent with Kiss et al. (2000)'s argument of cross-production [6]. The resulting cross-harmonic calculation is displayed in fig. 3.5. Considering this, each possible combination of periods from fundamental to 4th order was calculated, for which the python scheme can be seen in app. C. This process was then repeated for all masses of evolution; the results of this analysis is described in the following chapter.

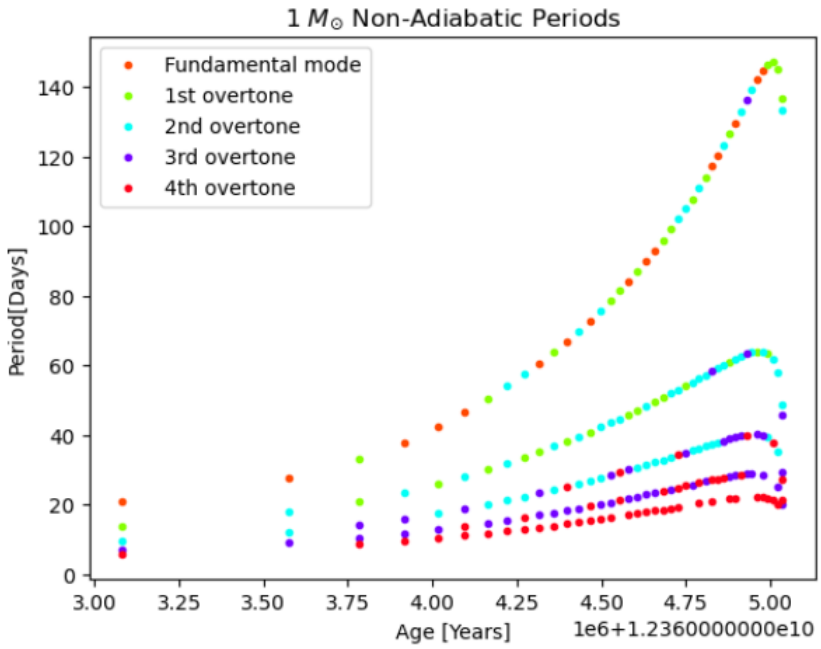

Figure 3.4: Result of adiabatic period calculations of a 1 $M_\odot$ star in the AGB region of evolution.

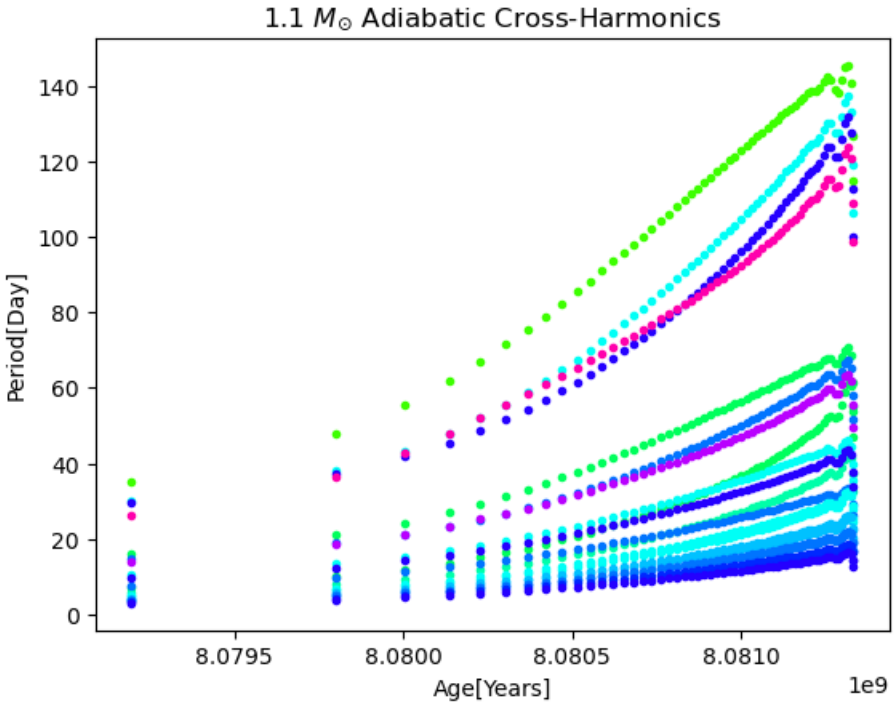

Figure 3.5: Result of cross-harmonics calculation of a 1 $M_\odot$ star in the AGB region of evolution.

Chapter 4

Results and Discussion

We now move to discuss the results in three parts and their implication. The first section will discuss the evolution tracks and the quality of the evolution models used to calculate the pulsation periods. The next part will discuss the calculated pulsation periods and their implications and evolution over time. The final part will discuss the cross-harmonic frequency calculations and whether they are a potential cause of LSPs. The potential for future research and shortcomings of this thesis will also be discussed as an additional section, followed by a summary of conclusions.

4.1 Evolution Tracks

After the first step of calculating the evolution tracks, we obtain 6 separate HRDs for each mass calculated. Figures 4.2 through 4.4 display each evolution track individually, while 4.1 displays all tracks together for easy comparison. Looking at fig. 4.1, there are many interesting features that do not persist in all evolution tracks. This could be due to a variety of reasons; each one will be discussed in order of increasing mass. Recall that only evolution data from the AGB region will be used to calculate periods using GYRE. Because of this, some interesting features are commented on, but become irrelevant for period calculations.

In fig. 4.2a, the 0.85 $M_{\odot}$ track has a long extended horizontal branch that is not observed in any other evolution track. This feature is especially distinguishable from other models in fig. 4.1. The reason for this is unclear; a few options could

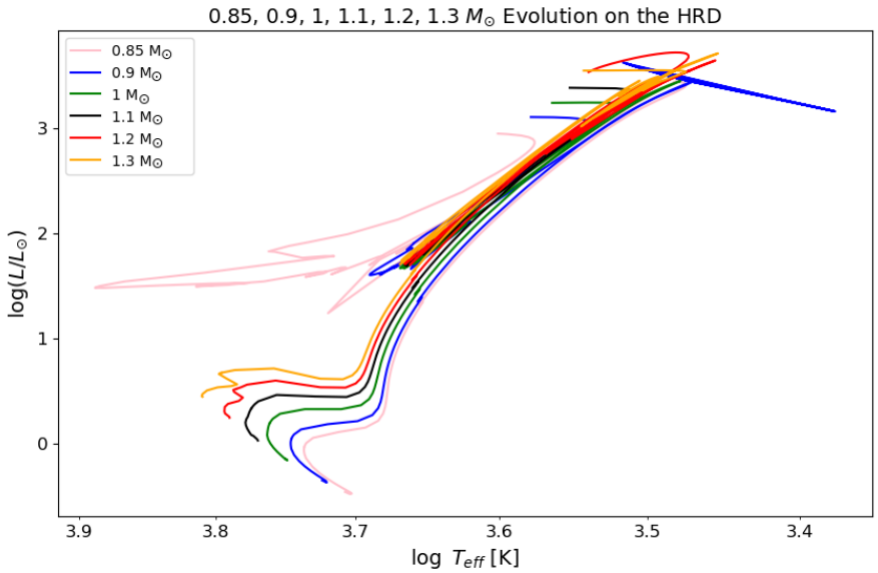

Figure 4.1: Evolution tracks 0.85, 0.9, 1, 1.1, 1.2, 1.3 $M_\odot$ displayed together on the HRD for the purpose of comparison.

explain this behaviour. The first option is that there is an unidentified issue with very low-mass calculations in MESA, and this feature is purely artificial. The next option could be that with the parameters used combined with the very low mass, we are in the regime of an extreme horizontal branch star (EHB). EHB stars are extremely hot stars that can travel to the far left regimes of the horizontal branch [29][30]. This is quite unlikely, as EHB stars are O-type stars, which means they are around 20,000-30,000 K and far out of the range of the model at hand [30]. Another reason this is unlikely is due to the origin of EHBs: currently the most accepted explanation is that these stars form in binary systems [30]. Obviously this would give our model no reason to become an EHB, and thus the likely culprit is a computational phenomenon. Exploring the reasoning behind this branch would require some computational knowledge of conducting stellar evolution models, and is left to future research. However the long horizontal branch does not occur in the AGB, and we are left with a seemingly normal AGB ascent for this mass. For this reason, we continue with the analysis of the 0.85 $M_\odot$ star.

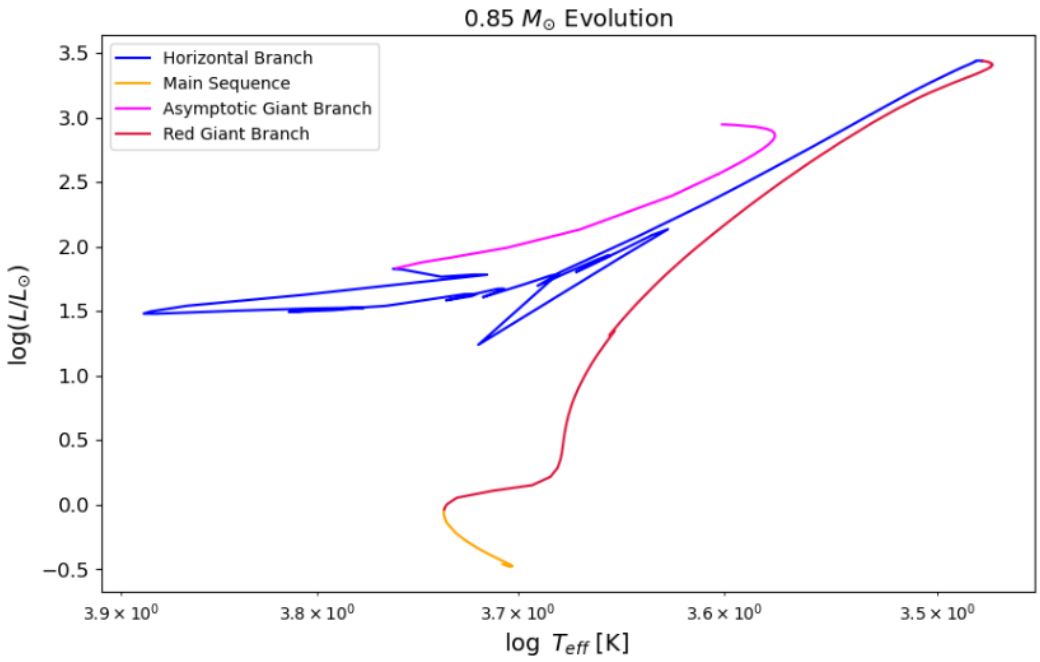

(a)

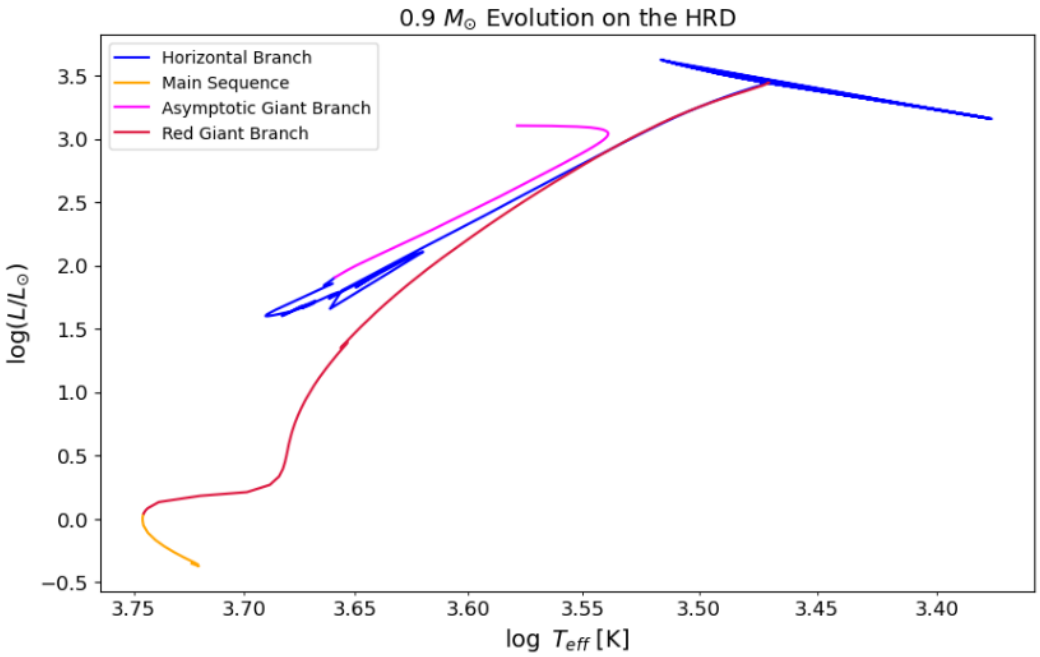

(b)

Figure 4.2: The evolution tracks of a 0.85 $M_\odot$ (a) and 0.9 $M_\odot$ (b) solar mass stars calculated using MESA

Comparatively, the evolution track of 0.9 $M_\odot$ given in fig. 4.13f looks much more "normal", except for a feature in the top right corner during He flash. This is a normal, real feature that only appears due to the timestep selection in this regime. Other masses also displayed this variation, but they did not get plotted due to the longer timesteps skipping over this region. The evolution is as expected and satisfactory for 0.9 $M_\odot$. This is also the case for the 1 $M_\odot$, 1.1 $M_\odot$, 1.2 $M_\odot$, and 1.3 $M_\odot$ solar mass stars given in fig. 4.3 through 4.4.

It is worth noting the messy-looking feature on the top right hand that occurs during the AGB phase for both 1.2 $M_\odot$ and 1.3 $M_\odot$ stars. This feature is likely a thermal pulse (TP) as mentioned during section 1.1. The behaviour during this phase will be further examined in 4.2. The next results that will be discussed is the calculation of the pulsation periods and the subsequent frequency calculation.

Some of the tracks also display a partial overlap between the AGB and end of the horizontal branch tracks. This is simply caused by "resuming" the MESA run from a point right before the AGB and is not a point of concern. The effects of performing the resume is further discussed in the next section.

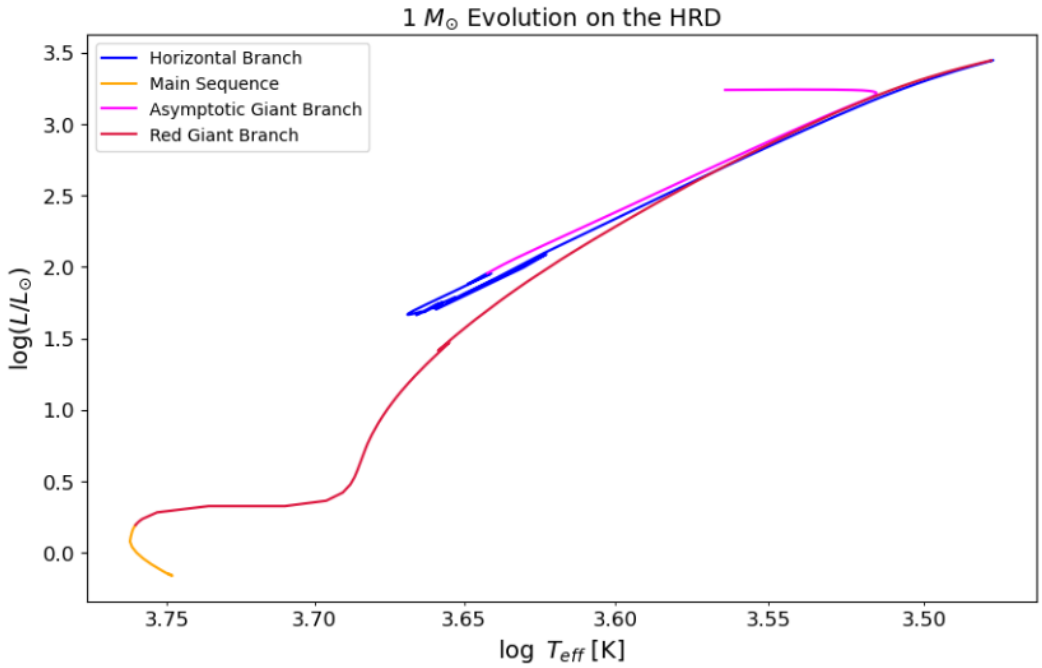

(a)

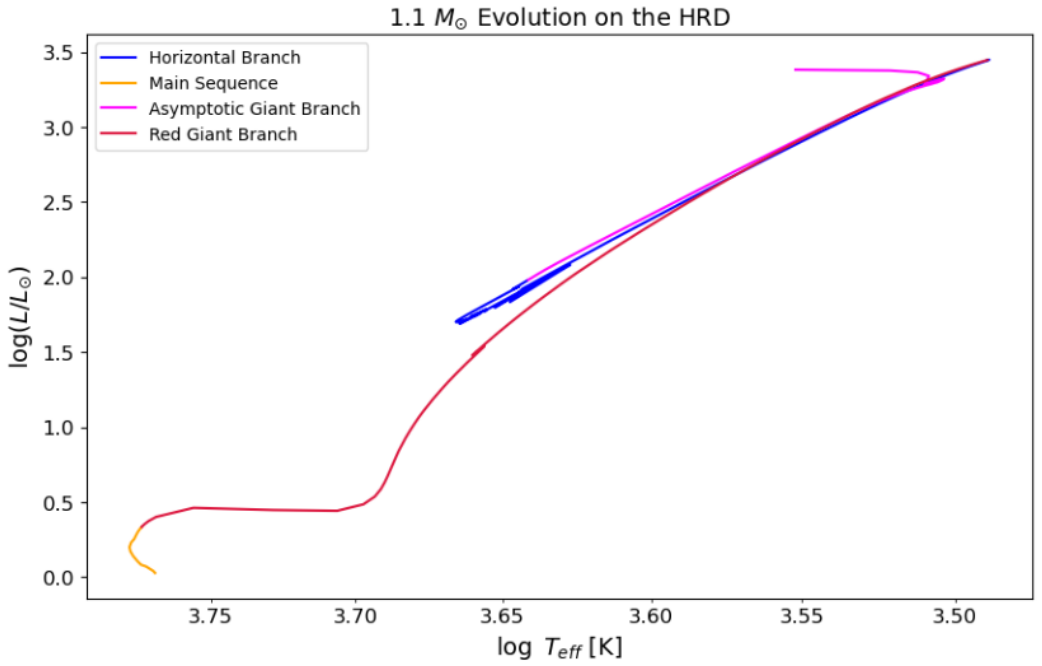

(b)

Figure 4.3: The evolution tracks of a 1 $M_\odot$ (a) and 1.1 $M_\odot$ (b) solar mass stars calculated using MESA

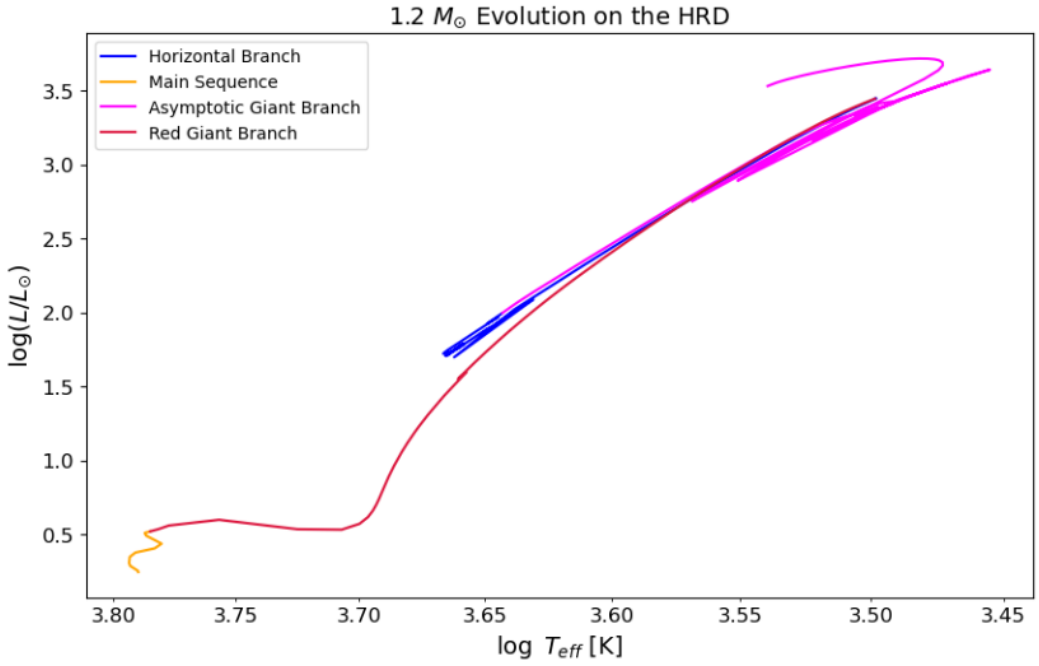

(a)

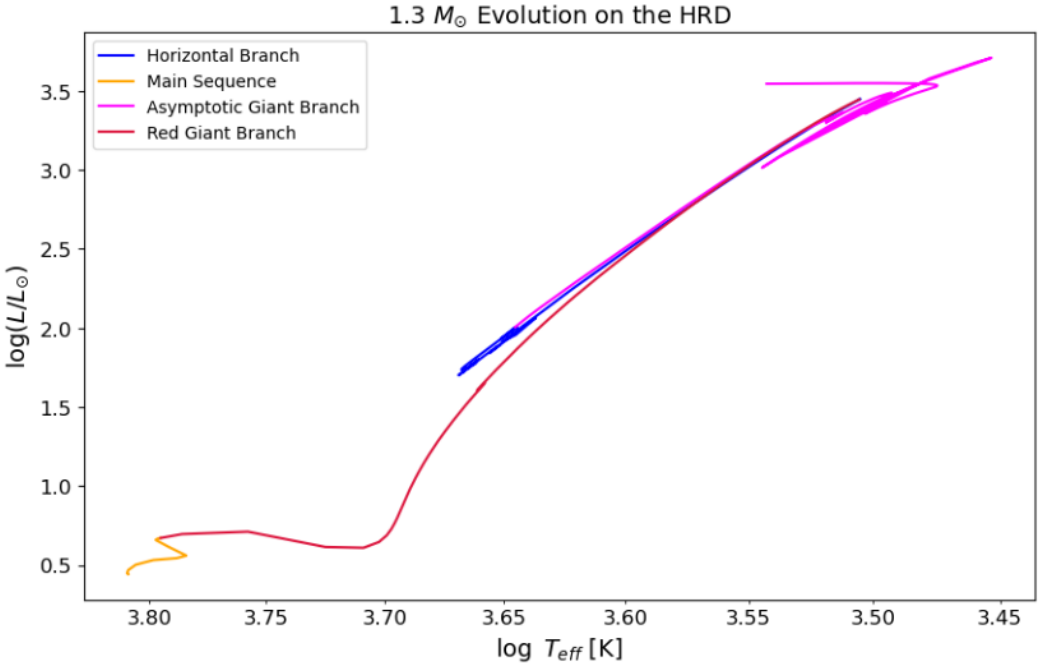

(b)

Figure 4.4: The evolution tracks of a 1.2 $M_\odot$ (a) and 1.3 $M_\odot$ (b) solar mass stars calculated using MESA

4.2 Pulsation Periods

After using MESA to calculate the evolution tracks and using the profiles to calculate the pulsation periods with GYRE, we are left with pulsation periods throughout each star's evolution on the AGB. Figures 4.11 through 4.11 display the result of adiabatic and non-adiabatic frequency calculations in the AGB region for each mass.

Beginning with 0.85 $M_{\odot}$, we observe a steady period increase in both the adiabatic and non-adiabatic cases. The difference between the two calculations is quite stark: for the adiabatic case, each mode is continuous, but this is not the case for the non-adiabatic periods. This condition is observed throughout all non-adiabatic cases from fig. 4.2a to 4.11. This could indicate an issue with root-finding for the non-adiabatic periods, as it looks like the correct periods are being calculated, but different modes are being assigned causing the abrupt discontinuity. Another interesting feature that comes with this is that the same modes are being reported simultaneously with different periods. All these factors contribute to a conclusion that non-adiabatic root finding needs further investigation. Additionally, as the mass of the model increases, the difference between the periods of the non-adiabatic and adiabatic modes increase. This is especially evident in the maximum frequency of fig. 4.11. While this does not result in a definite dismissal of the accuracy of the adiabatic calculations, it could indicate a need for re-examination. We leave this investigation up to future research, and continue with the analysis assuming the validity of adiabatic period calculations.

The next observation that needs to be addressed is large gaps in the period calculations for some of the masses. This is observed in the 0.9 $M_{\odot}$ and 1.3 $M_{\odot}$ period calculations. the most likely cause of this is the methodology: recall that during the AGB phase, the frequency of outputting a profile file was increased greatly, and the run resumed from the approximate switch point to the AGB regime. In doing so, selecting a starting point right before the beginning of AGB would mean the time step is much larger for the first few points until the AGB begins. Once the AGB begins and MESA start using the command in the AGB inlist, the time between outputs is greatly reduced. This is the reason for the large gaps, and is not an issue of concern for the accuracy of the period calculations. Fig. 4.11 (a) and (a) display the large gap, while (c) and (b) are zoomed in to the actual AGB region.

Continuing with the evaluation of each mass' period calculation, we consider the

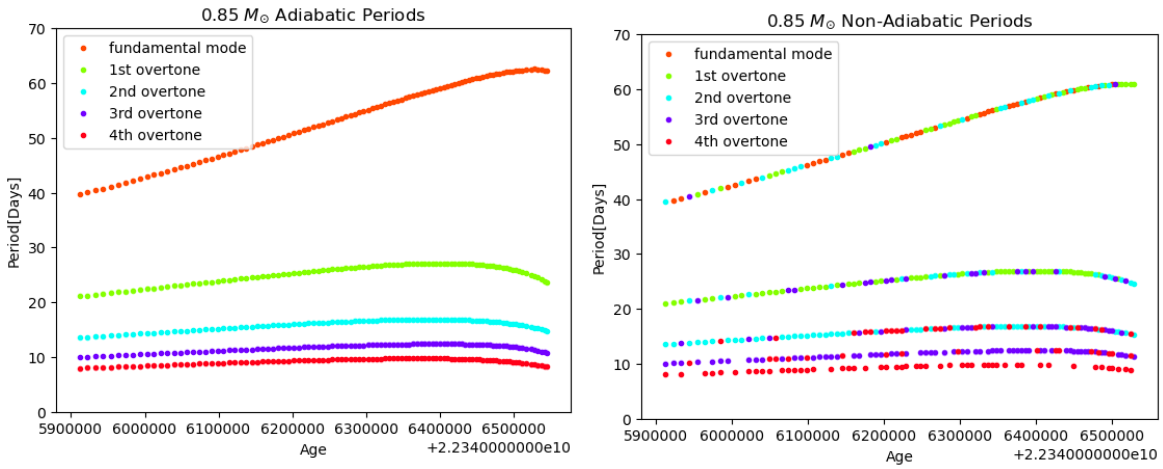

(a) (b)

Figure 4.5: The period calculations in the AGB region of a 0.85 $M_\odot$ star with adiabatic (a) and non-adiabatic (b) pulsations.

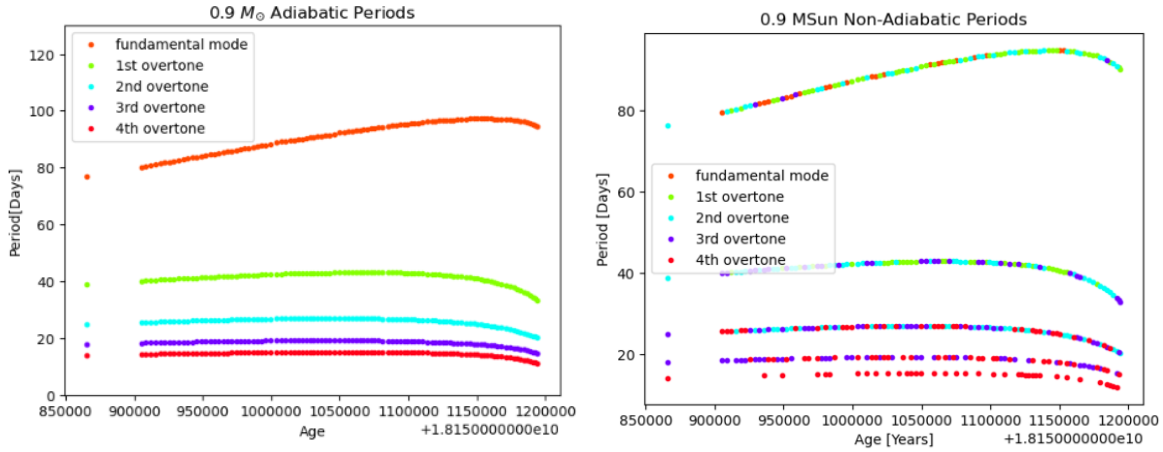

(a) (b)

Figure 4.6: The period calculations in the AGB region of a 0.9 $M_\odot$ star with adiabatic (a) and non-adiabatic (b) pulsations.

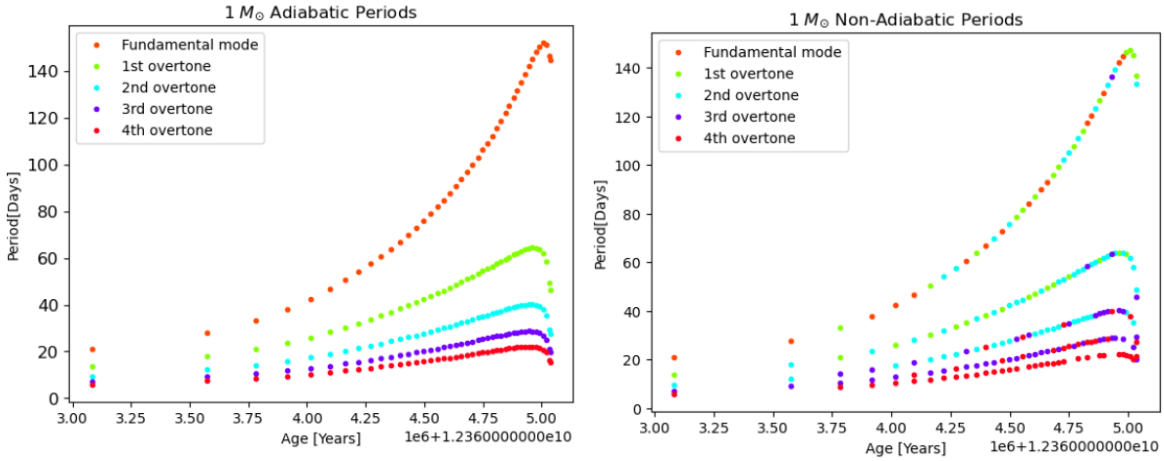

(a) (b)

Figure 4.7: The period calculations in the AGB region of a 1 $M_\odot$ star with adiabatic (a) and non-adiabatic (b) pulsations.

1 $M_\odot$ and 1.1 $M_\odot$ calculations. The period steadily increases before a sharp drop right before the end of the AGB phase. The reason for this abrupt drop is unclear, but could indicate the beginning of a thermal pulse that continues past the end of the MESA-defined AGB phase. In fact, all calculations abruptly cut-off when there is clearly still periodic behaviour past this point. Assuming periodicity must remain continuous and cannot display instantaneous changes, this indicates that periodicity continue past the point where we cut the calculation. The reason for this cut is because the stopping condition of "TPAGB" was used as a command for MESA, which can be seen in appendix A. This condition stops the run at the end of the AGB, which MESA defines as H-rich envelope mass below 10^{-2} $M_\odot$ [24]. This causes every run to terminate at a similar relative point as evidenced by fig. 4.1.

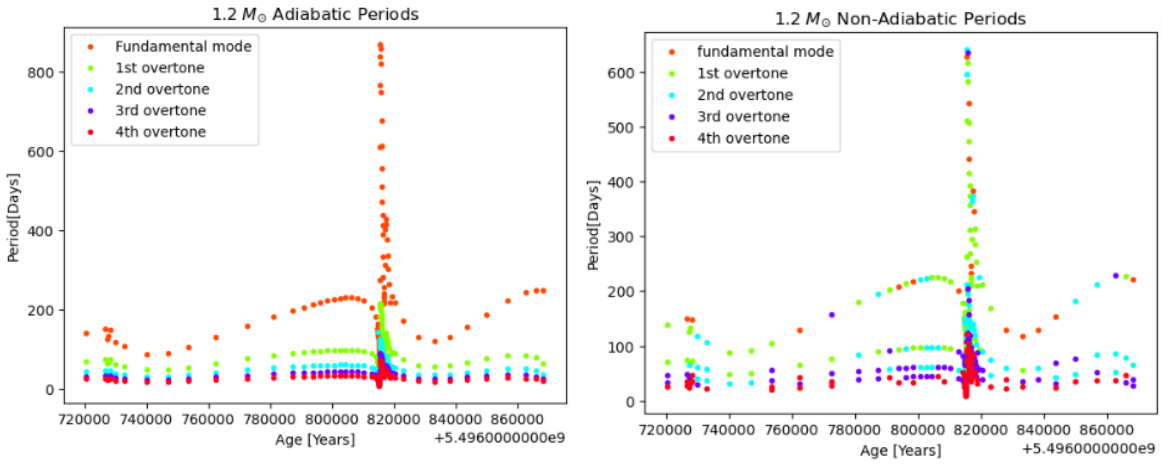

(a) (b)

Figure 4.9: The period calculations in the AGB region of a 1.2 $M_\odot$ star with adiabatic (a) and non-adiabatic (b) pulsations.

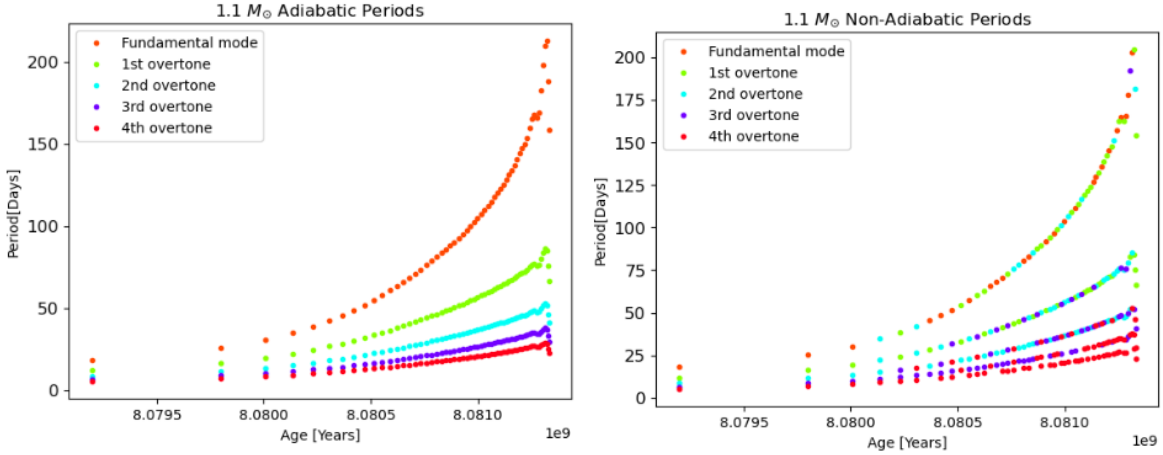

(a) (b)

Figure 4.8: The period calculations in the AGB region of a 1.1 $M_\odot$ star with adiabatic (a) and non-adiabatic (b) pulsations.

We see further evidence for thermal pulses in the 1.2 $M_\odot$ and 1.3 $M_\odot$ period calculations. In fig. 4.9, we observe a sharp spike indicating a sudden change in period lasting about 20000 years, which is consistent with the behaviour of a thermal pulse. We can compare this to a model of TPAGB period changes performed by Joyce et al. (2024), where they made a comprehensive characterization of the TPAGB star R Hydrae in order to fit observational data to theoretical data [31]. In doing so, they

present a figure of a computational model of a 1.5 $M_\odot$ star with solar metallicity, which is given in fig. 4.10 alongside the period calculations of this study. In comparing the overall shapes, this sudden change in the model we present is concluded to likely be a thermal pulse. This same argument is applied to our 1.3 $M_\odot$ model, where the enlarged region is given in fig. 4.13c. Both features in the 1.2 $M_\odot$ and 1.3 $M_\odot$ models are thus thermal pulses.

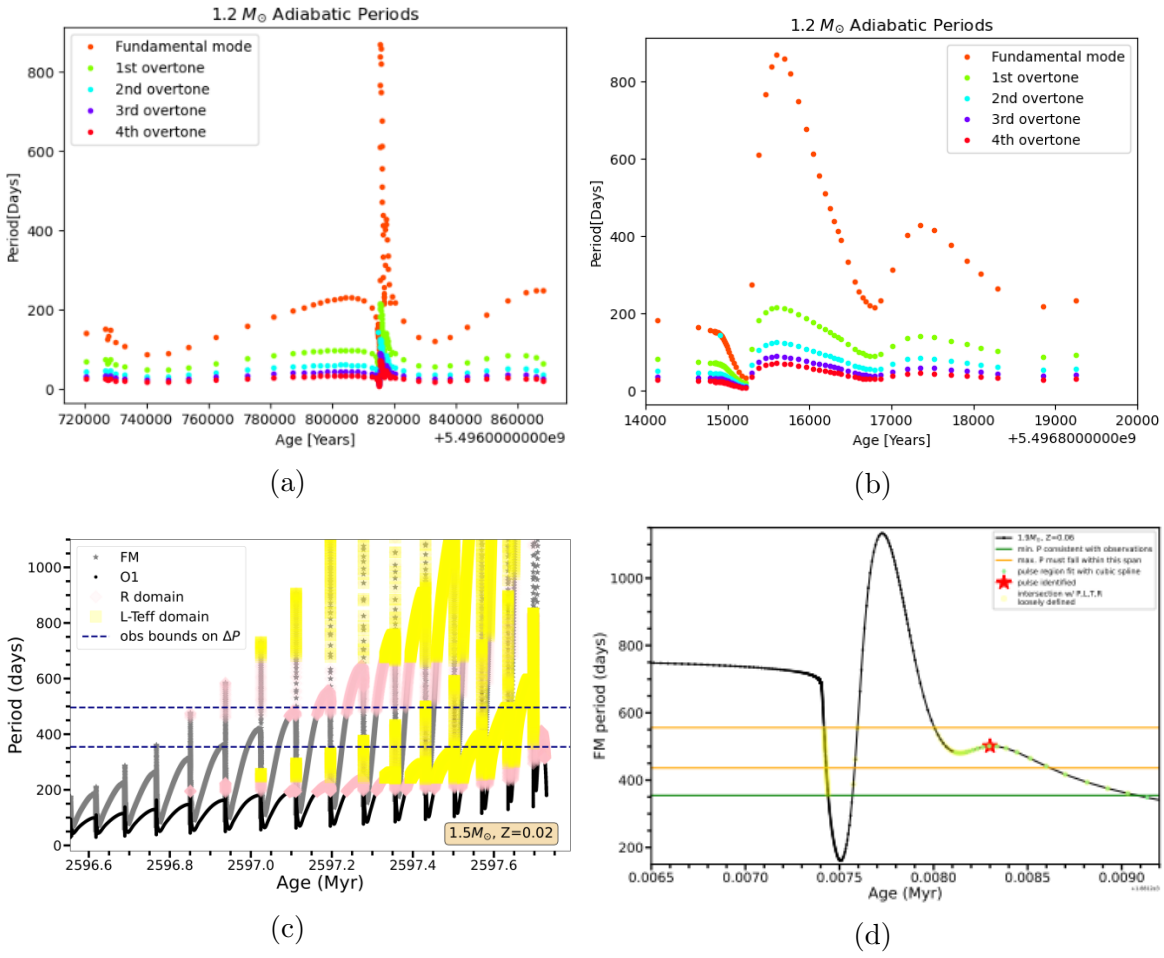

Figure 4.10: The adiabatic period calculations in the AGB region of a 1.2 $M_\odot$ star given in (a). The region of thermal pulse is then enlarged in (b). Figure 5 of Joyce et al. (2024) is given in (c), displaying a computational model of a 1.5 $M_\odot$ solar metallicity star's thermal pulses. Figure (d) is also from Joyce et al. (2024), and is included to show the shape of a single thermal pulse [31].

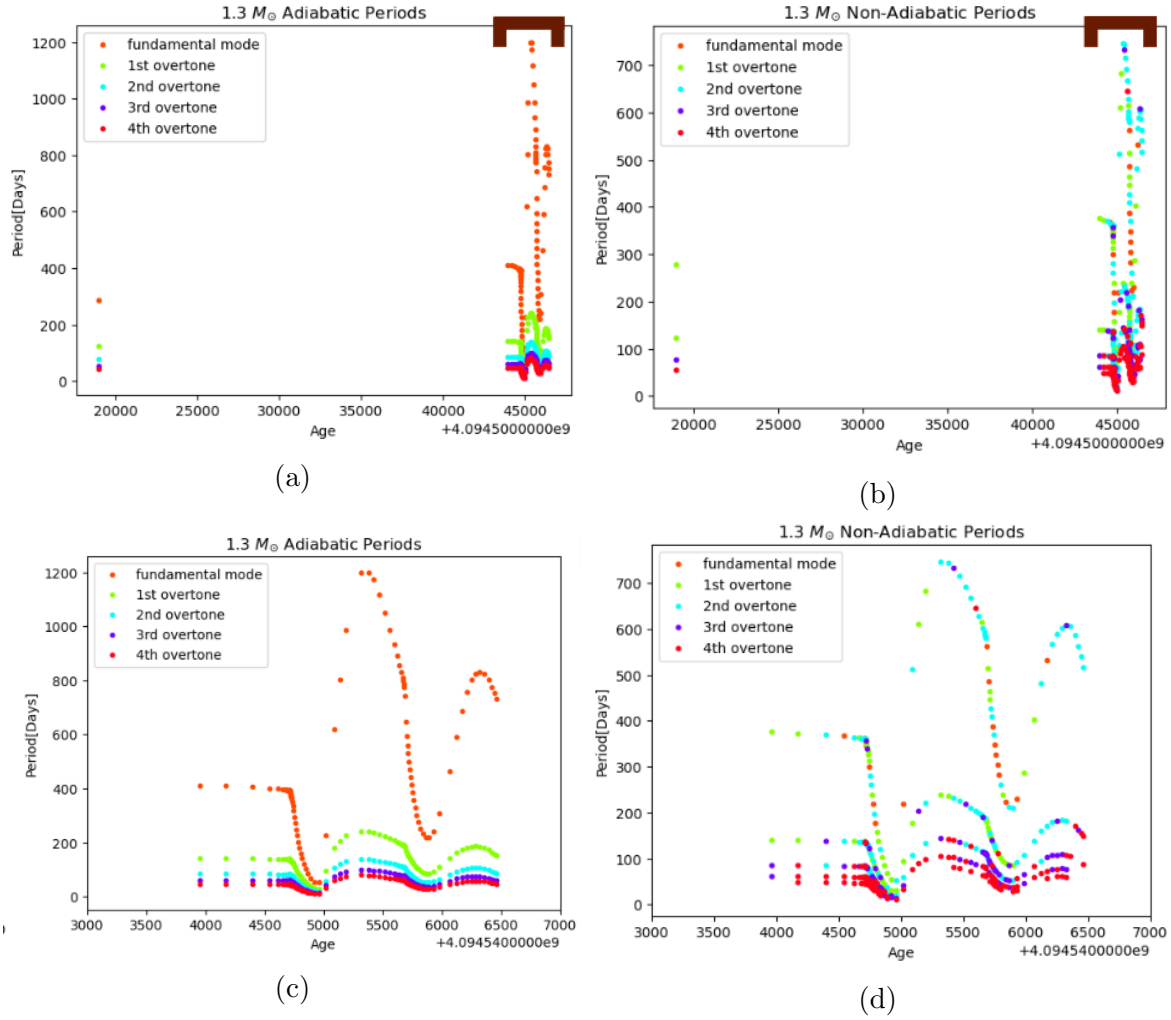

Figure 4.11: The period calculations in the AGB region of a 1.3 $M_\odot$ star with adiabatic (a) and non-adiabatic (b) pulsations. The highlighted regions in (a) and (b) are given in (c) and (d) respectively.

We can also make some comments about the period calculations when compared to the observational data discussed in section 2. The star V CVn by nature of being a multi-mode pulsator had two closely spaced periods at 192 and 186 days. In masses of 0.85 $M_\odot$ to 1.3 $M_\odot$ only the 1 $M_\odot$ and above masses achieve periods consistent with V CVn. Outside of thermally pulsing regions, no model displays two closely-spaced periods occuring simultaneously such as in V CVn. However, thermally pulsing regions so indeed display closely spaced period possibilities as the period is reaching a minima. We cannot definitively make conclusions about V CVn's mass or what part of pulsation it is in from this data as we do not have an upper mass limit that

caps how large V CVn could be. However, the observation that closely spaced periods only occur during thermally pulsing phases is interesting and worth considering the implications of. This is discussed further in section 4.4. Next we move to discuss the results of the cross-harmonic calculations.

4.3 Calculation of Cross-Harmonics

After applying the scheme given in appendix C for computing cross-harmonic periods, we obtain the graphs given in fig. 4.13 for all adiabatic cross-harmonics. The reason we leave out non-adiabatic periods is because of issues with the cross-harmonic calculation. This is demonstrated in fig. 4.12, where the non-adiabatic cross-harmonic periods are reduced to only a few points in time. This is the case for all non-adiabatic cross-harmonic calculations; they are not depicted in figures to avoid redundancy. The reason behind this is not fully clear, but comes from the cross-harmonic calculation code. The scheme only performs the cross-harmonic calculation if two modes occur at the exact same point in time to around the 5th decimal place in years. The likely explanation is that in the non-adiabatic calculation, the absence of some modes during some points in time is causing the code to not calculate the cross-harmonics at that point in time. While this is an issue with the code, this is not an issue caused by the computational model. The time requirements of this project did not allow for the correction of the cross-harmonic scheme, and is thus left for future research. We continue our analysis with the adiabatic cross-harmonic calculations.

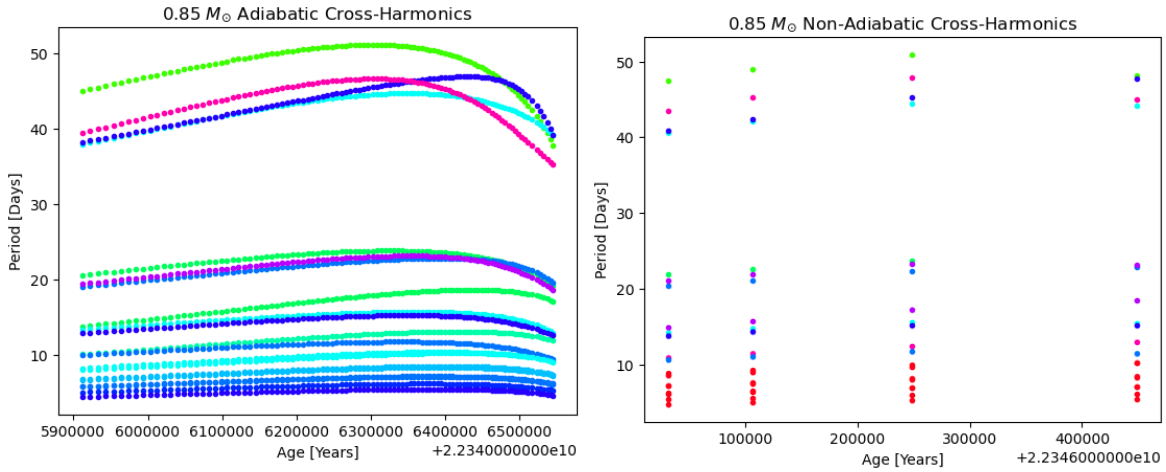

(a) (b)

Figure 4.12: The cross-harmonic period calculations in the AGB region of the 0.85 $M_\odot$ adiabatic model (a) and non-adiabatic model (b).

The first factor to check is whether we see a period 5-10 times any of the pulsation periods. The maximum cross-harmonic period occurs in the 1.3 $M_\odot$ model of 400 days, which is much shorter than the maximum pulsation period of the 800 day pulsation period in fig.4.11. In fact, all cross-harmonic periods are shorter than the maximum period of their corresponding pulsation period model. This makes sense when we consider the cross-harmonic formula from earlier:

$$f_{jk} = jf_1 + kf_2 \tag{4.1}$$

adding two frequencies will only cause a higher frequency, which corresponds to a shorter period. However, we cannot forget the Kiss et al (2000)'s formula of cross-production included both adding and subtracting the period. This still does not negate that the lowest frequency will always be lower than product of the lowest frequency subtracted from a different frequency. This also justifies only examining the case where $j = 1$ and $k = 1$, as any case where $j, k > 1$ will only increase the resulting frequency, decreasing the cross-harmonic period.

Next, keeping in mind that LPVs are categorized as having a pulsation frequency of 100 days or more, do we achieve any periods that are contenders for LSPs? Within the current standards of LPVs being between 5-10 times the main period, we would need a period of at least 500 to 1000 days. This automatically rules out the 0.85 $M_\odot$

and 0.9 $M_{\odot}$ models. The cross harmonics of the remaining models do show periods of > 100 days, but no periods between 500-1000 days.

This conclusion rules out the possibility of LSPs being caused by cross-harmonics for the models presented in this study. However, the original fundamental to 4th overtone models do indeed exhibit periods between 500 to 1000 days, and given that the average period of the model increases with mass, masses above 1.3 $M_{\odot}$ would display longer periods. Could these potentially be LSPs? We know that Mira variables oscillate in the fundamental mode, which would make them ineligible for the models presented here as the overtone periods are all shorter than the fundamental. SRVs do pulsate in first and second overtone modes, which could potentially mean that the LSP is caused by the longer, fundamental mode frequency. To be able to do this, we would need to know the main oscillation frequency, which is that of the highest amplitude. As mentioned previously, this is done by using non-adiabatic calculations of period to determine the growth and dampening rates of the oscillation modes. Given that we are unsure of the validity of the non-adiabatic calculations, this would require further research on modelling these pulsations non-adiabatically.

As a final note, we also are interested in the cause of V CVn's extra-long period of 5407 days. Given that a traditional LSP was not achievable with cross-harmonics, the possibility of an extra-long LSP is out of the question. However, should higher masses be investigated there is potential of achieving periods on the order of thousands of days. We observed fundamental mode pulsations of 1200 days with a 1.3 $M_{\odot}$ model, and the maximum period of pulsation are increasing with mass. However, this would require the star to be pulsating in the first or second overtone, and the LSP to be the fundamental mode. We can not make a conclusive statement on this due to the absence of the non-adiabatic calculations as explained previously.

4.4 Future Research Potential

Due to the time constraints of an undergraduate honours thesis, there were inevitably parts of this research that could have been explored but are left to future work for the sake of brevity. In this section, we briefly discuss aspects of this project that show considerable promise for future research in studying LSPs and cross-harmonics.

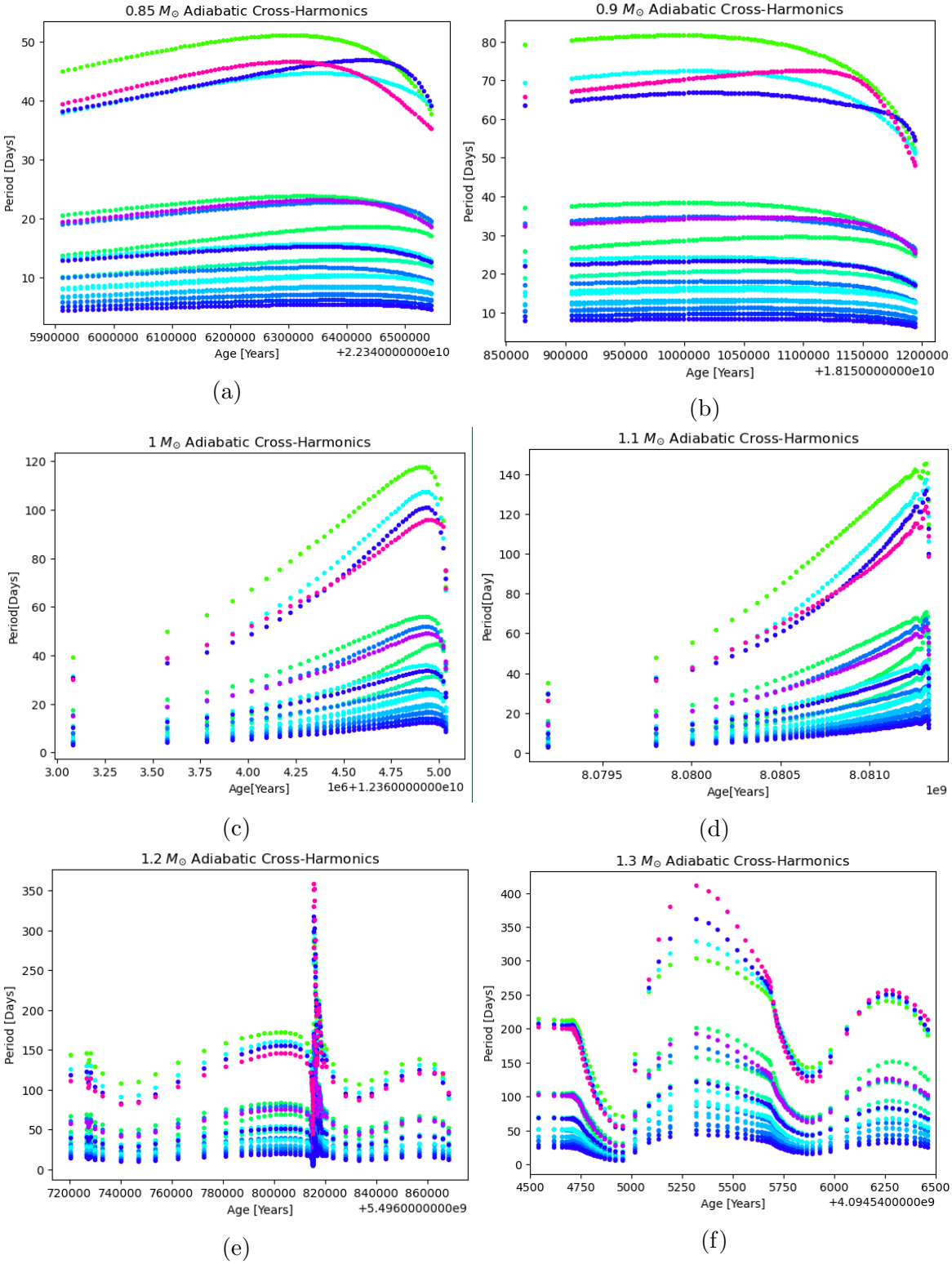

Figure 4.13: The adiabatic cross-harmonic calculations of 0.85 $M_\odot$ (a), 0.9 $M_\odot$ (b), 1 $M_\odot$ (c), 1.1 $M_\odot$ (d), 1.2 $M_\odot$ (e), and 1.3 $M_\odot$ (f).

The major aspect of this project that was left for future research was the non-adiabatic pulsation period calculation. While this does not deem this study obsolete, performing this analysis would solidify the conclusions of this study. As an example, obtaining non-adiabatic growth and dampening of the amplitudes of pulsation would allow for analyzing what mode the star is pulsating in at a given time. With this information, one would be able to then determine if LSPs could be a longer fundamental mode pulsation as mentioned in the previous section.

We also do not touch upon LPV period-luminosity (PL) sequences: LPVs are known to follow distinct PL sequences similar to Cepheid variables [32]. Different regions of this PL sequence correspond to different types of LPVs, with one specifically reserved for LPVs with long secondary periods [32]. Fitting models on this PL model could provide more insight into the model we use. Alongside this, not all LPVs display long secondary periods. This could be explained with an LSP corresponding to a thermal pulse as mentioned in the previous section, but further investigation is needed in population dynamics of LPVs in order to come to a conclusion about this.

Another aspect of analysis that would prove interesting results is performing these models for a larger mass range, and fitting observational brightness data of LPVs such as V CVn to the theoretical light curve. This analysis is similar to the analysis of Joyce et al. (2024) from [31]. This would mean obtaining luminosity vs. time data artificially with a high resolution, around 100 years, which is V CVn's recorded luminosity data length. MESA does have the capability of doing this, but obtaining the high-resolution luminosity vs. time data might prove difficult.

Finally, there are many stellar parameters we could vary such as metallicity and mass loss rate (wind) that could affect the periods of pulsation. We use uniform values across all models except for mass. Varying these parameters could provide more interesting conclusions, which is also a shortcoming of this thesis that we discuss next.

4.5 Shortcomings of this Thesis

The most obvious point of contention would be the adiabatic vs. non-adiabatic models of pulsation periods. As mentioned previously, the discrepancies between the two models do not discredit the adiabatic models, but the issue would need to be explained

or resolved before the findings can be presented as concrete evidence. Should the non-adiabatic model be dismissed as irrelevant, the difference in period calculations need to be explained and an error margin for adiabatic modelling needs to be introduced.

The next issue is discussed in the beginning of this thesis, and is related to the pulsation mechanism of LPVs. As mentioned, the interplay of pulsation and convection is not fully understood, and the exact mechanism driving LPV pulsation is unknown. In this model, we employ a general opacity mechanism while maintaining all other properties of LPV such as a large convective envelope and mixing length parameters, as well as mass loss rates and starting masses. Having an unknown pulsation mechanism, there is inevitably some differences that would arise from employing a scheme different from an opacity mechanism during the evolution tracks. The effects of different pulsation mechanisms should be investigated.

Finally, just as it is a potential for future research, not exploring the effects of varying mass loss rates and mixing length parameters leaves their effects open to interpretation. Only considering 6 mass regimes under hyper-specific conditions that is not necessarily reflective of LPV population dynamics. Changing any parameter could cause changes in the calculated periods and the subsequent cross-harmonics.

Chapter 5

Summary and Conclusions

Throughout this thesis, we have investigated potential of LSPs being caused by cross-harmonic periods during the AGB phase using the stellar modelling code MESA and the frequency calculation code GYRE. We begin by calculating the evolution tracks on the HRD of six mass models of 0.85 $M_{\odot}$, 0.9 $M_{\odot}$, 1 $M_{\odot}$, 1.1 $M_{\odot}$, 1.2 $M_{\odot}$, and 1.3 $M_{\odot}$. We then move on to using GYRE to calculate the pulsation frequencies for the AGB phase during which they become LPV stars. Once the pulsation frequencies are calculated we calculate the potential cross-harmonic periods to determine whether a long secondary period is achievable. Under the methods we use we do not observe any periods to be contenders for long secondary periods from the cross-harmonic calculations. We do not observe evidence for an extra-long secondary period such as the one observed in V CVn of 5407 days. However, we do observe periods that are consistent with traditional long secondary periods in the pulsation period calculations. For these periods to be an LSP, the star would need to be pulsating in the first or second overtone with the highest amplitude. Additionally, this phenomenon would need to be proved for all LSPs and not just specific conditions as used in this study.

Based on this, we reject the possibility of LSPs being caused by cross-harmonics only for the models presented in this study. The conditions of the model are too specific for the conclusion to be applied with a broad brush to all LPVs. These specific conditions are the mass range selected for modelling, the pulsation mechanism used, only considering the adiabatic case, and the non-exploration of varying parameters such as metallicity and mass loss. However, this does leave us with potential for future research that could lead to shows promising results.

Bibliography

[1] Bradley W. Carroll and Dale A. Ostlie. *An Introduction to Modern Astrophysics*. en. Google-Books-ID: PY0wDwAAQBAJ. Cambridge University Press, Sept. 2017. ISBN: 978-1-108-42216-1.

[2] Márcio Catelan and Horace A. Smith. *Pulsating Stars*. en. Google-Books-ID: tFhVDwAAQBAJ. John Wiley & Sons, Mar. 2015. ISBN: 978-3-527-40715-6.

[3] Conny Aerts. "Asteroseismology". In: *Physics Today* 68.5 (2015), pp. 36–42.

[4] Rudolf Kippenhahn, Alfred Weigert, and Achim Weiss. *Stellar Structure and Evolution*. en. Astronomy and Astrophysics Library. Berlin, Heidelberg: Springer Berlin Heidelberg, 2012. ISBN: 978-3-642-30255-8 978-3-642-30304-3. DOI: 10.1007/978-3-642-30304-3. URL: http://link.springer.com/10.1007/978-3-642-30304-3 (visited on 03/01/2024).

[5] C. Aerts, J. Christensen-Dalsgaard, and D. W. Kurtz. *Asteroseismology*. en. Astronomy and Astrophysics Library. Dordrecht: Springer Netherlands, 2010. ISBN: 978-1-4020-5178-4 978-1-4020-5803-5. DOI: 10.1007/978-1-4020-5803-5. URL: https://link.springer.com/10.1007/978-1-4020-5803-5 (visited on 02/19/2024).

[6] Laszlo L Kiss et al. "Multiperiodicity in semiregular variables-II. Systematic amplitude variations". In: *Astronomy and Astrophysics Supplement Series* 145.2 (2000), pp. 283–292.

[7] Da-Run Xiong and Li-Cai Deng. "Solar-like and Mira-like oscillations of stars—A uniform excitation mechanism". In: *Research in Astronomy and Astrophysics* 13.11 (2013), p. 1269.

[8] Michał Pawlak. "Do Miras show long secondary periods?" In: *Astronomy & Astrophysics* 669 (2023), A60.

[9] John R Percy. "Long Secondary Periods in Pulsating Red Giants: A Century of Investigation". In: *arXiv preprint arXiv:2209.09144* (2022).

[10] I Soszyński and A Udalski. "The light curve shapes as a key to resolving the origin of long secondary periods in red giant stars". In: *The Astrophysical Journal* 788.1 (2014), p. 13.

[11] Hideyuki Saio et al. "Oscillatory convective modes in red giants: a possible explanation of the long secondary periods". In: *Monthly Notices of the Royal Astronomical Society* 452.4 (2015), pp. 3863–3868.

[12] I Soszyński et al. "Binarity as the Origin of Long Secondary Periods in Red Giant Stars". In: *The Astrophysical Journal Letters* 911.2 (2021), p. L22.

[13] John R Percy and Mayank H Shenoy. "The Long Secondary Period (LSP) Variables: Overview and Some Analysis". In: *arXiv preprint arXiv:2312.05255* (2023).

[14] Galina Sherren, Hilding Neilson, and Abigale Cross. "An Investigation of Cross-Harmonics as the Cause of Long Secondary Periods in Long Period Variable Stars". In: *In Progress* (2024).

[15] David Benn. "Algorithms+ Observations= VStar". In: *Journal of the American Association of Variable Star Observers (JAAVSO)* 40.2 (2012), p. 852.

[16] B. K. Kloppenborg. *Observations from the AAVSO International Database*. 2023. URL: https://www.aavso.org.

[17] Grant Foster. *Analyzing Light Curves: A Practical Guide*. Lulu. com, 2010.

[18] Bill Paxton et al. "Modules for Experiments in Stellar Astrophysics (MESA): Pulsating Variable Stars, Rotation, Convective Boundaries, and Energy Conservation". In: *The Astrophysical Journal Supplement Series* 243 (July 1, 2019). ADS Bibcode: 2019ApJS..243...10P, p. 10. ISSN: 0067-0049. DOI: 10.3847/1538-4365/ab2241. URL: https://ui.adsabs.harvard.edu/abs/2019ApJS..243...10P (visited on 11/09/2023).

[19] Bill Paxton et al. "Modules for Experiments in Stellar Astrophysics (MESA): Convective Boundaries, Element Diffusion, and Massive Star Explosions". In: *The Astrophysical Journal Supplement Series* 234 (Feb. 1, 2018). ADS Bibcode: 2018ApJS..234...34P, p. 34. ISSN: 0067-0049. DOI: 10.3847/1538-4365/aaa5a8.

URL: https://ui.adsabs.harvard.edu/abs/2018ApJS..234...34P (visited on 11/09/2023).

[20] Bill Paxton et al. "Modules for Experiments in Stellar Astrophysics (MESA): Binaries, Pulsations, and Explosions". In: *The Astrophysical Journal Supplement Series* 220 (Sept. 1, 2015). ADS Bibcode: 2015ApJS..220...15P, p. 15. ISSN: 0067-0049. DOI: 10.1088/0067-0049/220/1/15. URL: https://ui.adsabs.harvard.edu/abs/2015ApJS..220...15P (visited on 11/09/2023).

[21] Bill Paxton et al. "Modules for Experiments in Stellar Astrophysics (MESA): Planets, Oscillations, Rotation, and Massive Stars". In: *The Astrophysical Journal Supplement Series* 208 (Sept. 1, 2013). ADS Bibcode: 2013ApJS..208....4P, p. 4. ISSN: 0067-0049. DOI: 10.1088/0067-0049/208/1/4. URL: https://ui.adsabs.harvard.edu/abs/2013ApJS..208....4P (visited on 11/09/2023).

[22] Bill Paxton et al. "Modules for Experiments in Stellar Astrophysics (MESA)". In: *The Astrophysical Journal Supplement Series* 192 (Jan. 1, 2011). ADS Bibcode: 2011ApJS..192....3P, p. 3. ISSN: 0067-0049. DOI: 10.1088/0067-0049/192/1/3. URL: https://ui.adsabs.harvard.edu/abs/2011ApJS..192....3P (visited on 11/09/2023).

[23] R. H. D. Townsend and S. A. Teitler. "GYRE: an open-source stellar oscillation code based on a new Magnus Multiple Shooting scheme". In: *Monthly Notices of the Royal Astronomical Society* 435.4 (Nov. 11, 2013), pp. 3406–3418. ISSN: 0035-8711, 1365-2966. DOI: 10.1093/mnras/stt1533. URL: https://academic.oup.com/mnras/article-lookup/doi/10.1093/mnras/stt1533 (visited on 03/20/2024).

[24] MESA Developers. *Modules for Evolution in Stellar Astrophysics*. Accessed: March 23, 2024. Year. URL: https://docs.mesastar.org/en/release-r24.03.1/index.html.

[25] Adam S. Jermyn et al. "Modules for Experiments in Stellar Astrophysics (MESA): Time-dependent Convection, Energy Conservation, Automatic Differentiation, and Infrastructure". In: *The Astrophysical Journal Supplement Series* 265 (Mar. 1, 2023). ADS Bibcode: 2023ApJS..265...15J, p. 15. ISSN: 0067-0049. DOI: 10.3847/1538-4365/acae8d. URL: https://ui.adsabs.harvard.edu/abs/2023ApJS..265...15J (visited on 11/09/2023).

[26] Gyre Developers. *Gyre User Guide Example Walkthrough*. Accessed: March 20, 2024. Year. URL: https://gyre.readthedocs.io/en/stable/user-guide/example-walkthrough.html.

[27] William Wolf and Josiah Schwaib. "PyMesaReader". In: (2017). URL: https://billwolf.space/py_mesa_reader/index.html#welcome-to-pymesareader-s-documentation.

[28] Rich Townsend and the PyGYRE Team. "The PyGYRE Package". In: (2020). URL: https://pygyre.readthedocs.io/en/latest/#the-pygyre-package.

[29] Noella Lambert d'Cruz et al. "The origin of extreme horizontal branch stars". In: *arXiv preprint astro-ph/9511017* (1995).

[30] Ulrich Heber. "Extreme horizontal branch stars". In: *arXiv preprint arXiv:0804.0507* (2008).

[31] Meridith Joyce et al. "Stellar Evolution in Real Time II: R Hydrae and an Open-Source Grid of¿ 3000 Seismic TP-AGB Models Computed with MESA". In: *arXiv preprint arXiv:2401.16142* (2024).

[32] Thomas Lebzelter et al. "Period-luminosity diagram of long period variables in the Magellanic Clouds-New aspects revealed from Gaia Data Release 2". In: *Astronomy & Astrophysics* 631 (2019), A24.

[33] M. Catelan. "Selected topics in the evolution of low-mass stars". en. In: *EPJ Web of Conferences* 43 (2013). Ed. by J. Montalbán, A. Noels, and V. Van Grootel, p. 01001. ISSN: 2100-014X. DOI: 10.1051/epjconf/20134301001. URL: http://www.epj-conferences.org/10.1051/epjconf/20134301001 (visited on 03/01/2024).

[34] J. Goldstein and R. H. D. Townsend. "The Contour Method: a New Approach to Finding Modes of Nonadiabatic Stellar Pulsations". In: *The Astrophysical Journal* 899.2 (Aug. 1, 2020), p. 116. ISSN: 0004-637X, 1538-4357. DOI: 10.3847/1538-4357/aba748. URL: https://iopscience.iop.org/article/10.3847/1538-4357/aba748 (visited on 03/20/2024).

[35] J. Goldstein and R. H. D. Townsend. "The Contour Method: a New Approach to Finding Modes of Nonadiabatic Stellar Pulsations". In: *The Astrophysical Journal* 899.2 (Aug. 1, 2020), p. 116. ISSN: 0004-637X, 1538-4357. DOI: 10.

3847/1538-4357/aba748. URL: https://iopscience.iop.org/article/10.3847/1538-4357/aba748 (visited on 03/20/2024).

[36] Icko Iben Jr. "Low mass asymptotic giant branch evolution. I". In: *Astrophysical Journal, Part 1, vol. 260, Sept. 15, 1982, p. 821-837.* 260 (1982), pp. 821–837.

Appendix A

MESA Code

The following code is taken from the adapted version of the "inlist to end agb" file of the "1M pre ms to wd" test suite that is available on default download of MESA. This file is used to evolve a 1 solar mass star on the main sequence through the AGB phase.

```
&star_job

      show_log_description_at_start = .false.

      load_saved_model = .true.
      load_model_filename = 'end_core_he_burn.mod'

      save_model_when_terminate = .true.
      save_model_filename = 'end_agb.mod'
      required_termination_code_string = 'envelope_mass_limit'


      change_D_omega_flag = .true.
      new_D_omega_flag = .true.

      pgstar_flag = .true.

/ ! end of star_job namelist

&eos

!Uses default regimes when left empty

/ ! end of eos namelist

&kap    Zbase = 0.02d0
```

```
      kap_file_prefix = 'gs98'
      use_Type2_opacities = .true.

/ ! end of kap namelist

&controls


      write_pulse_data_with_profile = .true.
      pulse_data_format='GYRE'

      envelope_mass_limit = 1d-2 ! Msun

      energy_eqn_option = 'eps_grav'
      use_gold2_tolerances = .true.

      num_trace_history_values = 2
      trace_history_value_name(1) = 'rel_E_err'
      trace_history_value_name(2) = 'log_rel_run_E_err'

      ! Adapt max_model_number to let simulation run long enough
      max_model_number = 20000


      stop_at_phase_TP_AGB = .true.     !Stopping condition to end at TPAGB phase

      am_nu_visc_factor = 0
      am_D_mix_factor = 0.0333333333333333d0
      D_DSI_factor = 0
      D_SH_factor = 1
      D_SSI_factor = 1
      D_ES_factor = 1
      D_GSF_factor = 1
      D_ST_factor = 1

      varcontrol_target = 1d-3
      delta_lgL_He_limit = 0.01d0

      cool_wind_full_on_T = 9.99d9
      hot_wind_full_on_T = 1d10
      cool_wind_RGB_scheme = 'Reimers'
      cool_wind_AGB_scheme = 'Blocker'
      RGB_to_AGB_wind_switch = 1d-4
      Reimers_scaling_factor = 0.8d0
      Blocker_scaling_factor = 0.7d0 ! 0.8d0
      initial_mass = 1.0     !Change this parameter for different masses
      initial_z = 0.02d0

      stop_at_phase_TP_AGB = .true.

      am_nu_visc_factor = 0
      am_D_mix_factor = 0.0333333333333333d0
      D_DSI_factor = 0
      D_SH_factor = 1
      D_SSI_factor = 1
```

```
      D_ES_factor = 1
      D_GSF_factor = 1
      D_ST_factor = 1

      varcontrol_target = 1d-3
      delta_lgL_He_limit = 0.01d0

      cool_wind_full_on_T = 9.99d9
      hot_wind_full_on_T = 1d10
      cool_wind_RGB_scheme = 'Reimers'
      cool_wind_AGB_scheme = 'Blocker'
      RGB_to_AGB_wind_switch = 1d-4
      Reimers_scaling_factor = 0.8d0
      Blocker_scaling_factor = 0.7d0 ! 0.8d0


! mixing

      ! the mixing used here is a demonstration of options, not a specific endorsement.
      ! for your own use, you should experiment with the options.

         use_other_mesh_delta_coeff_factor = .true.
         ! use xtra_coeff_os option.  see run_star_extras.

         mesh_dlog_pp_dlogP_extra = 0.25
         mesh_dlog_cno_dlogP_extra = 0.25

         mesh_dlog_3alf_dlogP_extra = 0.225
         mesh_dlog_burn_c_dlogP_extra = 0.225
         mesh_dlog_burn_n_dlogP_extra = 0.225
         mesh_dlog_burn_o_dlogP_extra = 0.225

         mesh_logX_species(1) = 'h1'
         mesh_logX_min_for_extra(1) = -6
         mesh_dlogX_dlogP_extra(1) = 0.25

         mesh_logX_species(1) = 'he4'
         mesh_logX_min_for_extra(1) = -6
         mesh_dlogX_dlogP_extra(1) = 0.25

         overshoot_scheme(1) = 'exponential'
         overshoot_zone_type(1) = 'any'
         overshoot_zone_loc(1) = 'any'
         overshoot_bdy_loc(1) = 'any'
         overshoot_f(1) = 0.014
         overshoot_f0(1) = 0.004

         T_mix_limit = 1d4

! output

      photo_interval = 50
      profile_interval = 1  !changed from 100
      history_interval = 10
      terminal_interval = 10
```

```
      write_header_frequency = 10


/ ! end of controls namelist



&pgstar




      Grid6_win_flag = .true.
      Grid6_win_width = 11

      !Grid6_file_flag = .true.
      Grid6_file_dir = 'png'
      Grid6_file_prefix = 'grid6_'
      Grid6_file_interval = 5 ! output when mod(model_number,Grid6_file_interval)==0
      Grid6_file_width = -1 ! (inches) negative means use same value as for window
      Grid6_file_aspect_ratio = -1 ! negative means use same value as for window

      Summary_Burn_xaxis_name = 'mass'
      Summary_Burn_xaxis_reversed = .false.
      Summary_Burn_xmin = 0.00 ! -101d0 ! only used if /= -101d0
      Summary_Burn_xmax = 2.1  ! only used if /= -101d0

      Abundance_xaxis_name = 'mass'
      Abundance_xaxis_reversed = .false.
      ! power xaxis limits -- to override system default selections
      Abundance_xmin = 0.00 ! -101d0 ! only used if /= -101d0
      Abundance_xmax = -101d0 ! only used if /= -101d0
      Abundance_log_mass_frac_min = -6 ! only used if < 0

      !Profile_Panels4_win_flag = .true.
      !Profile_Panels4_win_width = 6

      ! Abundance window -- current model abundance profiles

         !Abundance_win_flag = .true.

         Abundance_win_width = 9
         Abundance_win_aspect_ratio = 0.75 ! aspect_ratio = height/width

/ ! end of pgstar namelist
```

Appendix B

GYRE Code

B.1 Namelist for oscillation calculations

This is the namelist used to tell GYRE what parameters and controls to use to calculate the frequencies of a given model.

```
&constants
/

&model
  model_type = 'EVOL'  ! Obtain stellar structure from an evolutionary model
  file_format = 'MESA' ! File format of the evolutionary model
  file = 'profile1.data.GYRE' !make sure this is set to the first profile file in the model
/

&mode
  l = 0 ! Harmonic degree
/


&osc
  outer_bound = 'VACUUM' ! Assume the density vanishes at the stellar surface
  nonadiabatic = .TRUE.
/

&rot
/

&num
   diff_scheme = 'MAGNUS_GL2'
/

&scan
   grid_type = 'LINEAR'
```

```
   freq_min = 0.0001
   freq_max = 5.0
   freq_min_units = 'ACOUSTIC_DELTA'
   freq_max_units = 'ACOUSTIC_DELTA'
   n_freq = 200
/

&grid
  w_osc = 10 ! Oscillatory region weight parameter
  w_exp = 2  ! Exponential region weight parameter
  w_ctr = 10 ! Central region weight parameter
/


&ad_output
  summary_file = 'summaryA.h5'                          ! File name for summary file
  summary_item_list = 'l,n_pg,freq,freq_units,E_norm,M_star,L_Star' ! Items to appear in summary file
  detail_template = 'detail.l%l.n%n.h5'               ! File name template for detail files
  detail_item_list = 'l,n_pg,omega,x,xi_r,
                      xi_h,c_1,As,V_2,Gamma_1'        ! Items to appear in detail files
  freq_units = 'CYC_PER_DAY'                          ! Units of freq output items
/

&nad_output
summary_file = 'summaryNA.h5'                         ! File name for summary file
  summary_item_list = 'l,n_pg,freq,freq_units,E_norm,M_star,L_Star' ! Items to appear in summary file
  detail_template = 'detail.l%l.n%n.h5'               ! File name template for detail files
  detail_item_list = 'l,n_pg,omega,x,xi_r,
                      xi_h,c_1,As,V_2,Gamma_1'        ! Items to appear in detail files
  freq_units = 'CYC_PER_DAY'                          ! Units of freq output items
/
```

B.2 Bash script used to iterate through profile files

This is the bash script used to iterate through each profile file and output the frequency calculations as "summary" files. The controls for the given calculations are in a namelist file, given in the previous section. When executing this file, make sure that this bash script, the gyre.in namlist file, and all output files in a "profile.data.GYRE" format are in the same directory. Also ensure that the path of the namelist file is set to the correct namelist.

```
#!/bin/bash

# Define the path to your namelist file
gyre_in_file="/home/gsherren/Desktop/mesa_zipped/mesa-r23.05.1/star/1SolarMassGyre/1MmstoagbAGBGyre/gyre.in"
```

```
# Define the base name of the profile file
profile_base="profile"
#summaryA_base="summaryA"
#summaryNA_base="summaryNA"

# Define the number of profile files you have
num_profiles=5

# Loop through each profile number
for ((profile_num = 1; profile_num <= num_profiles; profile_num++)); do
    # Define the path to the current profile file
    profile_file="${profile_base}${profile_num}.data.GYRE"

    # Replace the profile file in gyre.in
    sed -i "s/file = 'profile[0-9]\+.data.GYRE'/file = '${profile_file}'/" "$gyre_in_file"

    # Run your program with the modified gyre.in file
    $GYRE_DIR/bin/gyre "$gyre_in_file"
    cp summaryA.h5 summaryA${profile_num}.h5
    cp summaryNA.h5 summaryNA${profile_num}.h5
done
```

Appendix C

Python Code for Plotting

This section goes through obtaining each plot for a 1 Solar Mass model. The plots obtained with the following code is an HRD, the periods for fundamental, 1st, 2nd, 3rd, and 4th overtones, and the mixed frequencies of each frequency combination.

The first code snippet yields the HRD:

```
#importing necessary packages
import matplotlib.pyplot as plt
import mesa_reader as mr
import numpy as np
import pandas as pd
import pygyre as pg
import os
import matplotlib.ticker as mticker
from matplotlib.ticker import ScalarFormatter

#Plotting the HRD for a 1 Solar Mass Star
h1 = mr.MesaData('/home/gsherren/Desktop/mesa_zipped/mesa-r23.05.1/star/test_suite/
1MmstoagbAGBprofs/LOGS_to_start_he_core_flash/history.data')
v1 = mr.MesaData('/home/gsherren/Desktop/mesa_zipped/mesa-r23.05.1/star/test_suite/
1MmstoagbAGBprofs/LOGS_to_end_core_he_burn/history.data')
k1 = mr.MesaData('/home/gsherren/Desktop/mesa_zipped/mesa-r23.05.1/star/test_suite
/1MmstoagbAGBprofs/LOGS_to_end_core_h_burn/history.data')
j1 = mr.MesaData('/home/gsherren/Desktop/mesa_zipped/mesa-r23.05.1/star/test_suite/
1MmstoagbAGBprofs/LOGS_to_end_agb/history.data')

logh1_Teff=(h1.log_Teff)
logv1_Teff=(v1.log_Teff)
logk1_Teff=(k1.log_Teff)
logj1_Teff=(j1.log_Teff)


#LOG files
logs1agb = mr.MesaData('/home/gsherren/Desktop/mesa_zipped/mesa-
```

```
r23.05.1/star/test_suite/1MmstoagbAGBprofs/LOGS/history.data')

logs1agb_Teff=(logs1agb.log_Teff)

fig, axes = plt.subplots()
fig.set_figwidth(6)
fig.set_figheight(6)

plt.plot(logv1_Teff,v1.log_L,label= "Horizontal Branch", color='b')
plt.plot(logk1_Teff,k1.log_L,label= "Main Sequence", color='orange')
plt.plot(logj1_Teff,j1.log_L,label= "Asymptotic Giant Branch", color='magenta')
plt.plot(logh1_Teff,h1.log_L,label= "Red Giant Branch",color='crimson')

###
plt.plot(logs1agb_Teff,logs1agb.log_L,label= "AGBextraprofs", color='k')
###

ax = plt.gca()

plt.gca().invert_xaxis()

plt.tick_params(axis='x', which='minor', labelsize=12)directory_paths = [
    '/home/gsherren/Desktop/mesa_zipped/mesa-r23.05.1/star/0.9SolarMassGyre/0.9MmstoagbStartHeFlashGyre/',
    '/home/gsherren/Desktop/mesa_zipped/mesa-r23.05.1/star/0.9SolarMassGyre/0.9MmstoagbCoreHeDepleteGyre/',
    '/home/gsherren/Desktop/mesa_zipped/mesa-r23.05.1/star/0.9SolarMassGyre/0.9MmstoagbAGBGyre/',
]
plt.tick_params(axis='y', which='major', labelsize=12)

plt.xlabel("$\log \ T_{eff}$ [K]", size = 14)
plt.ylabel("$\log(L/L_{\odot})$", size = 14)
plt.title("1 $M_{\odot}$ Evolution on the HRD", size = 14)

plt.xscale("log")
plt.legend( fontsize="10")


ax.xaxis.set_minor_formatter(mticker.ScalarFormatter())

plt.show()
```

Next, plotting the periods of 5 modes:

```
# Plot the results
cmap = plt.get_cmap('hsv')
for i in range(1, 6):
    for j in range(i + 1, 6):
        plt.plot(addsubage[f'{i}{j}'], 1/np.array(frequencysub[f'{i}{j}']), marker='.',
        linestyle='None', color=cmap((i + j) / 10), label=f'Fundamental Mode-1st Overtone')
        plt.plot(addsubage[f'{i}{j}'], 1/np.array(frequencyadd[f'{i}{j}']), marker='.',
        linestyle='None', color=cmap((i + j + 5) / 10), label=f'Fundamental Mode+1st Overtone')

plt.xlabel('Age[Years]')
plt.ylabel('Period[Days]')
```

```
plt.title('1 $M_{\odot}$ Adiabatic Frequency Operations')
plt.legend()
plt.show()
```

Finally, the calculation scheme for obtaining the mixed frequencies:

```
    #Calculating the mixed frequencies

# Initialize dictionaries to store results
addsubage = {f'{i}{j}': [] for i in range(1, 6) for j in range(i + 1, 6)}
frequencysub = {f'{i}{j}': [] for i in range(1, 6) for j in range(i + 1, 6)}
frequencyadd = {f'{i}{j}': [] for i in range(1, 6) for j in range(i + 1, 6)}

for age_idx, age_value in enumerate(age_listn[n_pg_filters[0]]):
    matching_indices = {n_pg_filter: np.where(np.array(age_listn[n_pg_filter]) == age_value)[0]
    for n_pg_filter in n_pg_filters}
    if all(matching_indices[n_pg_filter].size > 0 for n_pg_filter in n_pg_filters):
        for i in range(1, 6):
            for j in range(i + 1, 6):
                age_values_i = np.array(age_listn[i])[matching_indices[i]]
                age_values_j = np.array(age_listn[j])[matching_indices[j]]
                matching_age_indices = np.where(age_values_i == age_values_j)[0]
                if len(matching_age_indices) > 0:
                    addsubage_values = age_values_i[matching_age_indices]
                    frequencysub_values = np.abs(np.array(frequency_listsn[i])[matching_indices[i]]
                    [matching_age_indices] - np.array(frequency_listsn[j])[matching_indices[j]]
                    [matching_age_indices])
                    frequencyadd_values = np.abs(np.array(frequency_listsn[i])[matching_indices[i]]
                    [matching_age_indices] + np.array(frequency_listsn[j])[matching_indices[j]]
                    [matching_age_indices])
                    addsubage[f'{i}{j}'].extend(addsubage_values)
                    frequencysub[f'{i}{j}'].extend(frequencysub_values)
                    frequencyadd[f'{i}{j}'].extend(frequencyadd_values)
    else:
        for i in range(1, 6):
            for j in range(i + 1, 6):
                addsubage[f'{i}{j}'].append(np.NaN)
                frequencysub[f'{i}{j}'].append(np.NaN)
                frequencyadd[f'{i}{j}'].append(np.NaN)

# Plot the results
cmap = plt.get_cmap('hsv')
for i in range(1, 6):
    for j in range(i + 1, 6):
        plt.plot(addsubage[f'{i}{j}'], 1/np.array(frequencysub[f'{i}{j}']), marker='.',
        linestyle='None', color=cmap((i + j) / 10), label=f'Fundamental Mode-1st Overtone')
        plt.plot(addsubage[f'{i}{j}'], 1/np.array(frequencyadd[f'{i}{j}']), marker='.',
        linestyle='None', color=cmap((i + j + 5) / 10), label=f'Fundamental Mode+1st Overtone')

plt.xlabel('Age[Years]')
plt.ylabel('Period[Days]')
plt.title('1 $M_{\odot}$ Adiabatic Frequency Operations')
plt.legend()
plt.show()
```